Geomorphic complexity and sensitivity in channels to fire and floods in mountain catchments

Daniel J. Brogan [a], Lee H. MacDonald [b], Peter A. Nelson [a,*], Jacob A. Morgan [c]

[a] *Department of Civil and Environmental Engineering, Colorado State University, Fort Collins, CO 80523-1372, USA*
[b] *Department of Ecosystem Science and Sustainability, Colorado State University, Fort Collins, CO 80523-1476, USA*
[c] *Department of Civil and Environmental Engineering, University of Washington, Box 352700, Seattle, WA 98195-2700, USA*

ARTICLE INFO

ABSTRACT

Fires and floods are important drivers of geomorphic change. While the hydrologic and geomorphic effects of fires have been studied at the hillslope scale, we have much more limited data on post-fire runoff, channel changes, and inferred or measured sediment storage and delivery at larger scales. In this study we intensively documented channel changes over four years in two very similar ~15 km^2 catchments in the northern Colorado Front Range, Skin Gulch and Hill Gulch, that were burned primarily at high and moderate severity in June 2012. Ten and 11 cross sections and longitudinal profiles along the lower channel network were repeatedly surveyed in Skin Gulch and Hill Gulch, respectively. Summer thunderstorms generally caused deposition in the valley bottoms while incision resulted from the intervening baseflows and spring snowmelt, but a very high intensity summer thunderstorm in Skin Gulch just one week after burning caused much more deposition than in Hill Gulch. Fifteen months after burning both watersheds experienced an exceptional, long-duration flood resulting from a multi-day rainstorm with a several hundred year recurrence interval. This removed nearly all of the deposited post-fire sediment along with some of the older valley bottom deposits. The expansion and coarsening of the channel has greatly decreased the geomorphic sensitivity of both watersheds to future floods, and eliminated the more typical and persistent post-fire depositional signature. The channel changes in Skin Gulch after the fire and long-duration flood were much greater than in Hill Gulch, and this can be attributed to the much greater sediment deposition in Skin Gulch shortly after the fire, reduced geomorphic sensitivity in Hill Gulch resulting from a large erosional flood in 1976, and the spatial distribution of burn severity and storm rainfalls leading to lower peak flows in Hill Gulch. These results suggest that fires in the Rocky Mountains can trigger significant and dynamic hillslope and channel changes over sub-decadal timescales, but unusually long or intense rainstorms can cause larger and more persistent changes regardless of whether a catchment has recently burned.

© 2019 Published by Elsevier B.V.

1. Introduction

Fires and floods are of increasing concern given that global warming is leading to more wildfires (e.g., Rocca et al., 2014; Westerling et al., 2006) and a higher likelihood of extreme precipitation (Berg et al., 2013). Wildfires reduce ground and canopy cover, increase soil water repellency, decrease infiltration rates, and decrease surface roughness (DeBano et al., 1998; Ebel et al., 2012; Larsen et al., 2009; Moody et al., 2013; Onda et al., 2008; Scott and Wyk, 1990; Shakesby and Doerr, 2006). These changes greatly increase surface runoff and erosion rates (Benavides-Solorio and MacDonald, 2001; Benavides-Solorio and MacDonald, 2005; Johansen et al., 2001; Morris and Moses, 1987; Robichaud et al., 2000; Swanson, 1981; Wondzell and King, 2003), and induce rapid headward expansion of the channel network (Collins

and Ketcham, 2001; Wohl, 2013) and very high hillslope-stream connectivity (sensu Shahverdian, 2015; Sosa-Pérez and MacDonald, 2017).

Post-fire sediment produced from hillslopes can be substantial, but the headwater channel incision and downstream channel erosion can account for over 80% of the total eroded sediment from a burned watershed (e.g., Moody and Martin, 2001). In certain environments sediment can be evacuated from small tributaries by debris flows, but only if sufficient sediment is available (e.g., Florsheim et al., 1991; Wohl and Pearthree, 1991) and the combination of burn extent, soil properties, topography, and rainfall conditions are conducive to debris flows (Cannon et al., 2010). Eroded sediment from upstream sources can be transported downstream as suspended sediment, degrading water quality (e.g., Rhoades et al., 2011; Smith et al., 2011; Writer et al., 2014), and as bedload (Wagenbrenner and Robichaud, 2014), which can degrade aquatic habitat and adversely affect downstream infrastructure. Much of the sediment transported as bedload is deposited on alluvial fans and overbank on floodplains and terraces where slopes

* Corresponding author.
E-mail address: peter.nelson@colostate.edu (P.A. Nelson).

decrease and valleys widen (e.g., Meyer et al., 1992; Moody and Martin, 2004; Moody and Martin, 2009; Reneau et al., 2007). Wildfires therefore can engender a temporally and spatially complex response of erosion and deposition, depending on the spatial and temporal distribution of rainfall amounts and intensities (e.g., Laird and Harvey, 1986; Moody and Martin, 2001).

As vegetation regrows infiltration, erosion rates, and the channel network usually revert back to pre-fire conditions within one to three years (e.g., Benavides-Solorio and MacDonald, 2005; Larsen et al., 2009; Moody and Martin, 2001; Morris and Moses, 1987; Wohl and Scott, 2017). In contrast, downstream sediment deposits can persist for tens to possibly thousands of years (e.g., Cotrufo et al., 2016; Elliott and Parker, 2001; Legleiter et al., 2003; Meyer et al., 1992; Meyer et al., 1995; Moody and Martin, 2001). The contribution of sediment due to fires compared to long-term sediment yields has been shown to be around 30–50% (Meyer et al., 1995; Roering and Gerber, 2005), although this varies drastically depending on the environment (Swanson, 1981). Much of our understanding of wildfire effects on hydrologic and geomorphic processes is based on studies conducted at the plot to hillslope scales, so there remains a need to better quantify and understand fire effects at larger scales (Moody et al., 2013). The accurate prediction of watershed-scale sediment yields and geomorphic changes are critical to protect downstream landowners, water users, and aquatic resources, and guide post-fire rehabilitation treatments.

In both burned and unburned watersheds the downstream changes are driven by water and sediment inputs (Poff et al., 1997; Wohl et al., 2015), and we have much more information on the larger-scale geomorphic effects of floods in unburned watersheds (e.g., Fryirs, 2013; de Vente et al., 2007; Walling, 1983) than in burned watersheds (e.g., Moody et al., 2013). Smaller floods may do very little geomorphic work (e.g., Costa and O'Connor, 1995; Kochel, 1988; Magilligan et al., 1998), but by definition extreme floods typically generate very large increases in sediment yield (e.g., Erskine and Saynor, 1996) and cause significant geomorphic changes through erosion and deposition (e.g., Baker, 1977; Friedman and Lee, 2002; Krapesch et al., 2011; Magilligan et al., 2015; Miller, 1990; Nanson, 1986; Schumm and Lichty, 1963). Other than post-fire debris flows, there have been very few studies of extreme or long-duration floods following wildfire (e.g., Doehring, 1968; Hamilton et al., 1954). Both long-duration and wildfire-induced floods can cause significant geomorphic changes at the watershed scale, but we rarely have had the opportunity to directly compare these two types of floods to determine which has a greater impact on downstream channels and valley bottoms.

In this study, we quantified the geomorphic response of the channel networks in two watersheds that had a very different flood history prior to and then immediately after a severe wildfire in June 2012. One watershed was subjected to an extreme flood in 1976, while the other watershed was subjected to a very high-intensity summer thunderstorm just one week after burning that caused tremendous amounts of erosion and downstream deposition (Brogan et al., 2017). Fifteen months after the fire an extreme, multi-day rainstorm caused widespread flooding, erosion, and sedimentation in the Colorado Front Range (e.g., Gochis et al., 2014; Moody, 2016; Yochum, 2015; Yochum et al., 2017). In our watersheds, approximately two-thirds of the rainfall fell over a two-day period, and the resulting long-duration high flows caused extensive channel changes both in our two watersheds as well as throughout the Colorado Front Range, and this flood has been termed the 'mesoscale flood' (Gochis et al., 2014). Accurate stage or flow data are not available due to the large amounts of aggradation that took place during this flood.

The different magnitudes, duration, and sequence of floods in our two study watersheds allowed us to compare the response of each watershed to different post-fire storms and the subsequent mesoscale flood. It is well recognized that high and moderate severity wildfires can greatly increase the sensitivity of a watershed to perturbations (Swanson, 1981), where sensitivity is defined as "the propensity of a system to respond to a minor external change" (Schumm, 1998,

p. 78). Sensitivity also can vary across the landscape and over time depending on other previous perturbations (Fryirs, 2017; Thomas, 2001). In the absence of fires, the effects of floods will depend not only on the magnitude and duration of flows, but also the intrinsic and extrinsic thresholds of the channel and the availability of sediment, which are affected by the magnitude and timing and of previous floods (e.g., Baker and Costa, 1987; Brierley, 2010; Costa and O'Connor, 1995; Newson, 1980; Schumm, 1973; Wolman and Miller, 1960).

Our initial objective was to evaluate post-fire changes in erosion and deposition over time in the lower portions of the two study watersheds, and use this to help predict post-fire sediment storage and delivery. The long-duration mesoscale flood greatly altered the channel and valley bottom, particularly in Skin Gulch, so our study objectives expanded to: (1) compare the magnitude and variability of post-fire channel change to the channel changes resulting from and following the long-duration mesoscale flood; (2) evaluate how watershed history and post-fire conditions in the two watersheds affected the observed sequence of channel changes; and (3) develop a conceptual model to describe potential channel and valley bottom responses to fires and large floods. The results should help resource managers better predict the likely geomorphic changes from fires and floods at scales up to 10–20 km^2, and use this to help assess post-fire risks and management strategies.

2. Background and study area

Following the 2012 High Park Fire (HPF), we initiated channel monitoring in two ~15 km^2 watersheds, Skin Gulch (SG) and Hill Gulch (HG) (Fig. 1). We were not able to monitor an unburned control watershed due to the lack of a nearby comparable watershed as well as limitations of personnel and funding. Both SG and HG drain north into the Cache la Poudre River, which is the primary water supply for Fort Collins and other communities. Prior to burning, the main channels in SG and HG were ~1 m wide with ephemeral to intermittent flow. Elevations in SG range from 1840 to 2680 m, while elevations in HG, which is only about 8 km to the east, are slightly lower at 1720 to 2400 m (Fig. 1). SG and HG are very similar, with respective mean slopes of 23 and 24%, drainage densities of 2.5 and 2.3 km km^{-2}, and elongation ratios of 0.53 and 0.44. SG is underlain by knotted mica schist, amphibolite, and pegmatite with a large shear zone through the northwestern edge of the watershed (Abbott, 1970; Abbott, 1976), while HG is underlain primarily by knotted mica schist (Braddock et al., 1988). Soils are primarily Redfeather sandy loams with more frequent rock outcrops in HG than SG (Soil Survey Staff, 2018).

Mean annual precipitation is 450–550 mm (PRISM Climate Group, Oregon State University, http://prism.oregonstate.edu), with winter precipitation falling primarily as snow and thunderstorms predominating in the summer. Prior to burning, the vegetation in both watersheds was dominated by ponderosa pine with some lodgepole pine stands at higher elevations. Mountain shrub and grasslands occupied some of the lower elevation and south-facing slopes, and there were only scattered narrow bands of deciduous riparian trees and shrubs along some of the larger stream channels. About 65% of each watershed was burned at moderate to high severity. In SG, the areas burned at moderate and high severity were primarily in the upper watershed, while in HG, most of the more severely burned areas were in the lower portions of the watershed (Fig. 1a). Following the fire, both streams became perennial.

3. Methods

3.1. Data collection

Our primary data are repeated field surveys of channel cross sections (XS) and corresponding longitudinal profiles (LP) in the lower portions of the two study watersheds (Fig. 1). XSs and LPs were established from early July to mid-October 2012, and monitoring continued until
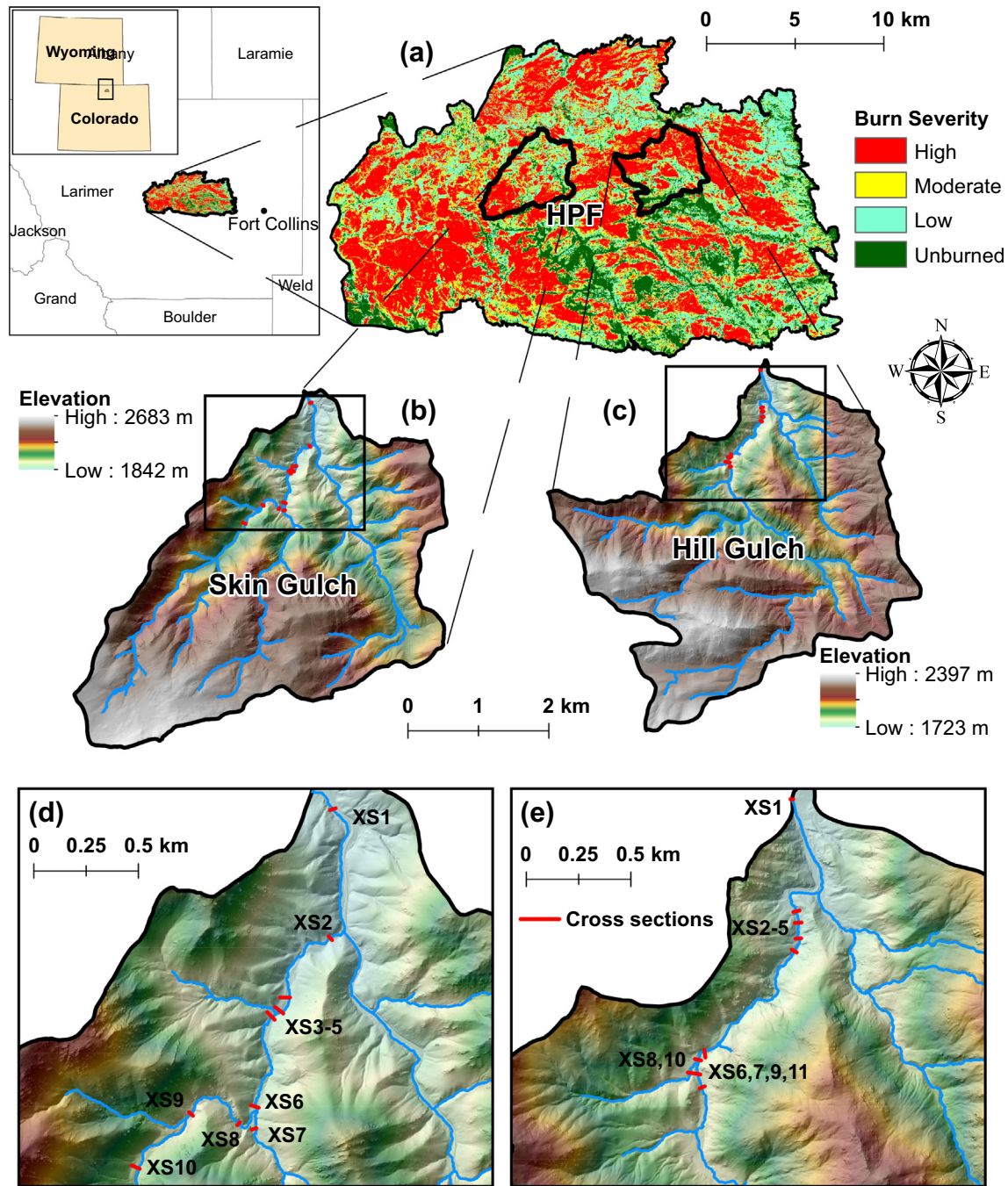
Fig. 1. (a) Location and burn severity of the High Park Fire (HPF) in the Colorado Front Range of the western U.S.A. Elevation maps of (b) Skin Gulch and (c) Hill Gulch. Black boxes in (b) and (c) indicate the areas that include the ten and eleven cross sections shown in (d) Skin Gulch and (e) Hill Gulch, respectively.

November 2016. Ten XSs were established in SG and eleven in HG at scales ranging from ~1 to 15 km^2, and sequentially numbered starting at the lowest XS (Fig. 1). The XSs were established in reaches that we anticipated—based on local geomorphic characteristics such as slope, width, and confinement—would represent a range of geomorphic responses from primarily erosional to primarily depositional. Because the XSs were selected to focus on specific processes rather than as a random or systematic sample, the site-specific results cannot be extrapolated to longer reaches or the entire watershed. Since the first large thunderstorm occurred in SG only one week after the fire, the only pre-storm data in either watershed was the initial survey of XS1 in SG which, in hindsight, was too short to include all of the resulting deposition.

Each XS was monumented with rebar and surveyed from 15 to 25 times over the five-year study period, while the monumented LPs

were surveyed from 10 to 21 times. Each survey is uniquely identified by the XS or LP number and the collection date using the format of yyyymmdd (e.g., 20120912). Upstream, downstream, and cross-stream photos were taken during the site visits. Some of the initial surveys in summer 2012 used an autolevel and stadia rod, while a Leica TCR407 total station was used in fall 2012. Starting in spring 2013, a TOPCON GR-5 real-time kinematic Global Navigation Satellite System (RTK-GNSS) was typically used to survey topography from monumented benchmarks in each watershed, but an autolevel and stadia rod were occasionally used in summer 2013. Autolevel and total station surveys were rotated and translated to match RTK-GNSS coordinates based on local benchmarks that we established. Mean horizontal and vertical root mean square errors for the RTK-GNSS data were 6 mm and 10 mm, respectively, and these values were assumed to be

valid for the other survey methods given that they were matched to the RTK-GNSS coordinates. No data were available for XS1 in SG after September 2013 as the accumulated sediment was mechanically removed and a new channel was constructed.

After the September 2013 mesoscale flood, we surveyed 42 and 51 high water marks (HWMs) in SG and HG, respectively. The HWMs were identified primarily by matted down vegetation and deposits of litter or other fine debris. The uncertainty in the elevations of the surveyed HWMs was estimated to be no more than 0.10 m, and this is similar to the uncertainties used in other indirect discharge analyses (e.g., Brogan et al., 2017; Moody, 2016). Eleven HWMs in SG and 32 HWMs in HG were used to calibrate a two-dimensional model for estimating peak flows as described below.

Pebble count data (Wolman, 1954) were collected in June/July 2013 and in February/March 2014 at each XS, and these bracketed the mesoscale flood (a second sample could not be collected at XS1 in SG due to the sediment removal and channel reconstruction). The pebble counts were conducted across the channel as identified by either the edge of vegetation or newly-formed sediment deposits. From 97 to 280 particles were measured in each case (mean = 139). At XS8 in HG, the deposited sediment was too fine to determine the median and D_{84} particle sizes, so a 4-L grab sample was collected, air dried, sieved in 1/2-phi increments, and weighed.

Airborne laser scanning (ALS) surveys were collected by the National Ecological Observatory network (NEON) Airborne Observation Platform in July 2013, and jointly by the U.S. Geological Survey (USGS) and the Federal Emergency Management Agency in October 2013. We used 1-m resolution bare-earth digital elevation models (DEM) from these two surveys to develop the two-dimensional model for estimating peak flows from the 2013 mesoscale flood in each watershed.

Historic aerial photos were used to evaluate the channel changes in the downstream portion of SG and HG prior to and after the 1976 flood, and these were supplemented with photographs and an interview from a homeowner in lower HG who directly observed this flood. Precipitation isohyets for the 1976 storm were developed from data provided by MetStat Inc. These different sources of data allowed us to compare the channel and floodplain changes from the 1976 flood to the observed and measured changes following the 2012 HPF and the 2013 mesoscale flood.

3.2. Data analysis

The contributing area for each cross section was computed from the October 2013 1-m DEM. Valley widths at each cross section were delineated using 2-m contours created from the DEM, aerial imagery, our photographs, and field observations.

The XS and LP data varied in plan view (XY space) due to both channel migration and the exact placement of the survey rod. To maximize the accuracy of the calculated elevation changes for each XS, all of the X and Y data from all surveys for a given XS were plotted and a linear regression was developed to provide a best estimate of the XS location; each survey point was then orthogonally projected onto the linearly regressed XS. This process eliminates the false changes in elevation resulting from variations in the point-to-point summations of cross stream distances or surveyed elevations that were not exactly on the cross section.

An active channel width was defined for each XS based on the maximum extent of channel changes over the study period. Elevation differences among the different surveys were calculated by interpolating elevations every centimeter across the active channel for each XS, and then computing the elevation difference for each one-centimeter interval. Trapezoids were calculated for the elevation differences between surveys and summed to compute positive area (total deposition), negative area (total erosion), net change, and total absolute change. The mean elevation change of the active channel due to the mesoscale flood was calculated as the mean elevation difference between the last pre-flood and first post-flood surveys. The change in thalweg elevation

for each XS due to the mesoscale flood was calculated as the difference in the minimum elevation between the last pre-flood and first post-flood surveys.

The mean absolute elevation difference (MAED; i.e., the mean of the absolute values of the elevation differences every centimeter across the active channel width) was computed for each successive XS survey, and this is referred to as the variability in the cross sections. For each XS and LP the median MAED was calculated using all of the XS and LP surveys prior to and after the mesoscale flood, and this characterized the absolute magnitude of variability for the pre- and post-flood time periods, respectively. Because the channel bed was composed primarily of gravels and cobbles, there was some inherent variability in the surveys due to the exact placement of the survey rod relative to these grains. Hence, we compared the MAED to one half of the local D_{84} grain size (i.e., the diameter coarser than 84% of the measured particles), and this helped us evaluate whether the computed elevation changes (MAED) were larger than the inherent grain-scale variability in our topographic surveys.

The mean length of the longitudinal profiles was 120 m with a range of 74 to 244 m. Similar to the cross sections, the longitudinal profiles were projected onto a hand-delineated polyline that best represented the average centerline over time. At some sites, two to four XSs were close enough to be included in a single LP. In these cases, the LP began downstream of the lowest XS (e.g., XS3 of XS3–5 in SG, and XS2 of XS2–5 in HG). By projecting the LP data onto a common channel centerline, the elevation changes along the LPs from successive surveys could be compared in the same manner as described previously for the XSs. Local slopes for each LP were estimated using a linear regression (Scott et al., 2016) for roughly 50-m long segments of the LPs clipped around each XS. Most of the LP segments were centered on the XSs, but if tributary confluences were nearby the LP was asymmetrical to avoid any slope breaks due to the confluence. Mean change in elevation due to the mesoscale flood was computed as the mean elevation difference along the length of each LP (or allocated portion of a LP if the LP crossed more than one XS) between the last pre-flood and first post-flood LP surveys. MAED was also computed for each LP, or portion of the LP relevant to a given XS, for each successive survey.

The NEON DEM from July 2013 required translation in order to register with the USGS DEM and our field data. Using our own Python script we calculated differences in slopes and aspects between the NEON DEM and the USGS DEM (following Nuth and Kääb, 2011), and these differences were used to estimate the required XYZ translation to best match the NEON DEM to the USGS DEM. This process was repeated until the translation changes in X, Y, and Z were <1 cm, or the required shift for that iteration was <2% of the overall shift. Vertical comparison of the DEMs with RTK-GNSS measurements indicated mean absolute

Table 1
Cross section (XS) contributing areas and valley widths for Skin Gulch and Hill Gulch. The * indicates that the valley width for cross section 1 in HG is the width of the much wider alluvial fan rather than the width of the relatively confined channel. † and ‡ denote pairs of cross sections that were surveyed along the same transect and share the same valley width.

XS	Skin Gulch		Hill Gulch	
	Area (km²)	Valley width (m)	Area (km²)	Valley width (m)
1	15.4	40	14.4	110*
2	9.0	22	11.2	16
3	8.8	44	11.1	25
4	8.8	55	11.1	23
5	8.3	38	11.1	21
6	8.1	40	10.7	36
7	2.8	21	10.2	49†
8	5.2	13	0.4	49†
9	5.1	26	10.2	68‡
10	4.6	38	0.4	68‡
11	n/a	n/a	10.2	33

elevation differences of 16 cm and 9 cm for the NEON ALS and USGS ALS, respectively.

Peak flows during the mesoscale flood were estimated using Nays2D following the procedure described by Brogan et al. (2017). Nays2D is a two-dimensional hydrodynamic model distributed with the International River Interface Cooperative (iRIC; http://i-ric.org; Nelson et al., 2016), which computes water surface elevations and depth-averaged velocities by solving the 2D depth-averaged equations of fluid continuity and momentum. Peak flows were estimated by minimizing the mean absolute error (MAE) between the elevation of the surveyed HWMs and the modeled water surface elevations. Peak flows were estimated for both the pre-flood and post-flood channel topography as determined from the pre- and post-flood lidar datasets because of the extensive channel incision and widening that occurred during this flood (see Brogan et al., 2017 for further details on this approach).

4. Results

Contributing drainage areas for the different cross sections ranged from 2.8 to 15.4 km^2 in SG and 0.4 to 14.4 km^2 in HG (Table 1). Valley widths varied from 13 to 55 m in SG and 16 to 68 m in HG, with the exception that at XS1 in HG the 15-m-wide armored channel is set into a 110-m-wide alluvial fan (Table 1). In HG, two pairs of XSs (XS7 and XS8, and XS9 and XS10) were surveyed along one long transect as these XSs were on two different tributaries just upstream of a confluence; hence the XSs in each pair have the same valley width (Table 1). Channel slopes ranged from 4 to 10% in SG (Table 2) and 1–7% in HG (Table 3), indicating that the majority of our sites would have been classified as step-pool or cascade prior to the fire (Montgomery and Buffington, 1997).

Cross section and longitudinal profile changes from two locations in SG (Fig. 2) and HG (Fig. 3) are representative in showing three distinct periods with different magnitudes and directions of channel geomorphic change. The first period is the initial post-fire response from summer 2012 through summer 2013, and this had varying amounts of both deposition and erosion due to summer thunderstorms and spring snowmelt. The second, relatively short period is the channel change due to the mesoscale flood. The third period is the subsequent two years of monitoring after the mesoscale flood when again there was both deposition and erosion, but on a much more smaller scale than in the first period (Tables 2 and 3). The following sections summarize the key XS and LP changes in each watershed over the different time periods in response to the sequence of rainstorms and snowmelt. Tables 2 and 3 summarize the quantitative changes in the XSs and LPs for each cross section, and plots of all of the surveys for each XS and LP are provided in the supplemental material.

4.1. Pre-mesoscale flood

4.1.1. Summer 2012

Convective thunderstorms caused extensive hillslope erosion and downstream deposition in the first summer after the fire. Quantitative data are largely lacking other than at XS1 in each watershed as the first storms occurred before we could set up the XSs and LPs, but at least 0.2 m of aggradation occurred at XS1 in SG and this aggradation extended well beyond the initial XS1 (supplemental Fig. S1). We also were able to document 0.5 m of aggradation at XS1 in HG as this XS also was installed in early July (Fig. 3a).

Frequent field visits occurred in summer 2012 in conjunction with the installation of sediment fences, and from these and the XS1 data in each watershed it is very clear that the greatest channel changes during this first period occurred just one week after the fire in SG as a result of a very intense rainstorm in the upper watershed over an area of high burn severity. The resulting peak flow was estimated at 20–46 m^3 s^{-1} km^{-2}, although this may be an overestimate as we did not account for any sediment bulking. Subsequent field observations indicated that this high-

Table 2
Geomorphic changes pre- and post-mesoscale flood for each cross section (XS) and longitudinal profile (LP) in Skin Gulch, including: mean change in elevation, change in thalweg elevation, approximate width of flood impact, median mean absolute elevation difference (MAED) between each successive XS survey both pre- and post-mesoscale flood, mean slope pre- and post-mesoscale flood, mean change in LP elevations, median MAED for each successive LP survey pre- and post-mesoscale flood, and key observations. Units are meters (m) except the mean LP slopes are in percent.

XS	Cross sections					Longitudinal profiles					Key observations	
	Mean change in elevation pre- to post-flood	Change in thalweg elevation from flood	Width of flood impact	Median MAED Pre-flood	Post-flood	Pre-mean slope (s.d.)	Post-flood mean slope (s.d.)	Mean change in elevation pre- to post-flood	Median MAED Pre-flood	Post-flood	Cross sections	Longitudinal profiles
1	0.79	0.72	31	0.05	0.06	4.1 (0.1)	4.2 (0.1)	0.95	0.18	0.06	Substantial deposition due to the mesoscale flood, but then altered with heavy machinery	Substantial deposition due to the mesoscale flood, but then altered with heavy machinery
2	−0.11	−0.10	17	0.08	0.04	3.9 (0.5)	6.3 (0.1)	−0.04	0.20	0.04	Frequent but minor changes	Headward knickpoint migration led to an increase in slope
3	−0.04	−1.16	14	0.17	0.06	6.6 (0.3)	7.3 (0.1)	−0.91	0.13	0.05	Channel shifted and incised down to bedrock	Uniform drop in bed elevation
4	−0.43	0.32	30	0.07	0.06	6.4 (0.3)	7.2 (0.1)	−0.02	0.13	0.05	Substantial channel widening with floodplain erosion and a slight increase in thalweg elevation	Slight increase in slope
5	−0.42	−0.37	20	0.06	0.05	6.4 (0.4)	4.8 (0.0)	−0.25	0.10	0.04	Channel shifted and incised with slight widening	Drop in bed elevation with slight decrease in slope
6	−0.38	−1.23	19	0.10	0.04	7.6 (0.5)	6.6 (0.1)	−0.62	0.28	0.05	Channel narrowed and incised	Drop in bed elevation with slight decrease in slope
7	−0.23	−0.48	4	0.05	0.04	10.4 (0.1)	8.2 (0.4)	−0.63	0.05	0.05	Channel widened and incised	Downstream end of profile remained fixed while the rest of the bed elevation decreased, leading to a decrease in slope
9	−0.33	−0.33	11	0.08	0.06	7.1 (0.4)	7.0 (0.2)	−0.53	0.17	0.05	Decrease in bed elevation	Uniform drop in bed elevation
10	−0.55	−1.14	8	0.07	0.07	8.1 (0.8)	9.2 (0.3)	−0.98	0.20	0.07	Slight channel shift and substantial incision	Uniform drop in bed elevation with a lot of exposed bedrock

Table 3
Geomorphic changes pre- and post-mesoscale flood for each cross section (XS) and longitudinal profile (LP) in Hill Gulch, including: mean change in elevation, change in thalweg elevation, approximate width of flood impact, median mean absolute elevation difference (MAED) between each successive XS survey both pre- and post-mesoscale flood, mean slope pre- and post-mesoscale flood, mean change in LP elevations, median MAED for each successive LP survey pre- and post-mesoscale flood, and key observations. Units are meters (m) except the mean LP slopes are in percent.

XS	Cross sections					Longitudinal profiles					Key observations	
	Mean change in elevation pre- to post-flood	Change in thalweg elevation from flood	Width of flood impact	Median MAED Pre-flood	Median MAED Post-flood	Pre-flood mean slope (s.d.)	Post-flood mean slope (s.d.)	Mean change in elevation pre- to post-flood	Median MAED Pre-flood	Median MAED Post-flood	Cross sections	Longitudinal profiles
1	0.32	0.38	5	0.04	0.04	1.1 (0.2)	1.9 (0.4)	0.62	0.05	0.05	Deposition led to an increase in thalweg elevation	Rise in bed elevation with slight increase in slope
2	0.03	0.04	5	0.07	0.04	5.1 (0.1)	4.2 (0.1)	0.11	0.12	0.04	No real change	Slight decrease in slope
3	0.02	0.12	7	0.06	0.05	3.7 (0.1)	4.2 (0.1)	0.00	0.08	0.04	No real change	No real change
4	−0.16	−0.06	8	0.07	0.05	3.3 (0.2)	3.3 (0.1)	−0.06	0.08	0.04	Slight widening of channel	No real change
5	−0.10	0.01	13	0.09	0.06	2.7 (0.2)	3.7 (0.1)	−0.21	0.11	0.04	Erosion on right bank offset by deposition on left bank	Increase in slope due to downstream incision
6	−0.04	−0.01	5	0.07	0.04	5.4 (0.2)	5.6 (0.1)	−0.15	0.07	0.04	No real change	No real change
7	−0.05	−0.13	4	0.07	0.06	5.2 (0.1)	4.2 (0.0)	−0.22	0.12	0.03	Minor channel incision	Decrease in slope due to upstream incision
8	−0.01	−0.10	6	0.08	0.03	7.1 (0.5)	7.4 (0.2)	−0.33	0.11	0.04	Ephemeral channel incised	Uniform drop in bed elevation
9	−0.06	−0.05	4	0.08	0.05	2.9 (0.1)	3.7 (0.1)	−0.09	0.07	0.03	No real change	Almost 1 m of incision at downstream end, otherwise no real change
10	−0.08	0.04	3	0.10	0.05	6.9 (0.2)	7.2 (0.1)	−0.15	0.07	0.03	No real change	No real change
11	−0.04	−0.15	6	0.06	0.03	3.4 (0.0)	3.1 (0.1)	−0.08	0.06	0.03	No real change	No real change

intensity storm caused tremendous hillslope and lower-order channel erosion that then caused very extensive downstream deposition, including 1-m imbricated boulders (Brogan et al., 2017). Subsequent thunderstorms caused smaller peak flows in both watersheds with additional sediment deposits and some reworking of previously deposited material. Much of the deposited sediment, other than the coarse material deposited from the first storm in SG, was relatively fine gravel and coarse sand, and this created relatively flat cross sections (e.g., Fig. 4a). Although deposition in HG was particularly evident at XSs 1, 7, 8 and 10, our observations and photos indicate that HG did not experience nearly the rainfall intensities, hillslope erosion, and downstream deposition that was evident from the first high-intensity convective storm in SG.

4.1.2. Winter 2012–2013

The summer deposits remained largely intact through the winter as the upper portions of both watersheds accumulated snow. Higher flows during spring snowmelt generated little or no hillslope erosion (Schmeer, 2014), while downstream flows caused varying amounts of channel incision through the post-fire deposits in both watersheds (e.g., Fig. 4). This incision was typically in a relatively narrow channel compared to the much wider sediment deposits. In some cases, exposed roots indicated that incision cut through the pre-fire streambed as well as the post-fire deposits. The mean thalweg elevation change in SG between September 2012 and May 2013 was −19 cm (s.d. = 22 cm), with a maximum incision of 60 cm at XS1 and a maximum aggradation of only 3 cm at XS7. There was less change in HG and the estimated mean thalweg elevation change over the same period was +5 cm (s.d. = 15 cm), but our field observations indicate that this apparent increase was at least partly caused by registration errors with the total station in fall 2012.

4.1.3. Summer 2013

In summer 2013, convective thunderstorms again caused extensive hillslope erosion (Schmeer et al., 2018) and downstream deposition in both watersheds (Figs. 2 and 3). Baseflows between storms incised through the finer sediments, while subsequent stormflows reworked and sometimes added to the sediment deposits in the channels. The overall pattern of channel changes in summer 2013 was similar to those in summer 2012, but changes were more frequent given the more frequent stormflows compared to the drier summer of 2012. While the mean thalweg elevation change in SG was only +2 cm (s.d. = 14 cm) and only −2 cm (s.d. = 9 cm) in HG, there was tremendous variability among the XSs in each watershed with maximum thalweg elevation changes of +71 cm in SG and +59 cm in HG.

Taken together, the survey data prior to the mesoscale flood indicate considerably larger changes and more variability in SG than HG (Fig. 5; Tables 2 and 3). For example, the average change in cross-sectional area in SG prior to the pre-mesoscale flood was 1.38 m², which is nearly double the mean change of 0.71 m² in HG. Mean elevation changes along the LPs were generally greater than the mean elevation changes for the XSs, and the LP changes in SG were around 5–10 cm greater than in HG (Fig. 5b and d).

4.2. Mesoscale flood of September 2013

Mean rainfall for the mesoscale flood was 260 mm in SG and 280 mm in HG, with maximum 15-min intensities of 33 mm h⁻¹ in both watersheds (Kampf et al., 2016). Stage measurements indicate that unusually high flows occurred for about 24 h in both watersheds (c.f. Kampf et al., 2016), but discharge over this period could not be accurately calculated because of the large changes in the channel XSs at the downstream stage recorders.

The sustained high flows caused much larger and more consistent XS and LP changes than were measured prior to the mesoscale flood (e.g., Figs. 2 and 3; Tables 2 and 3). Nearly all of the sediment that had
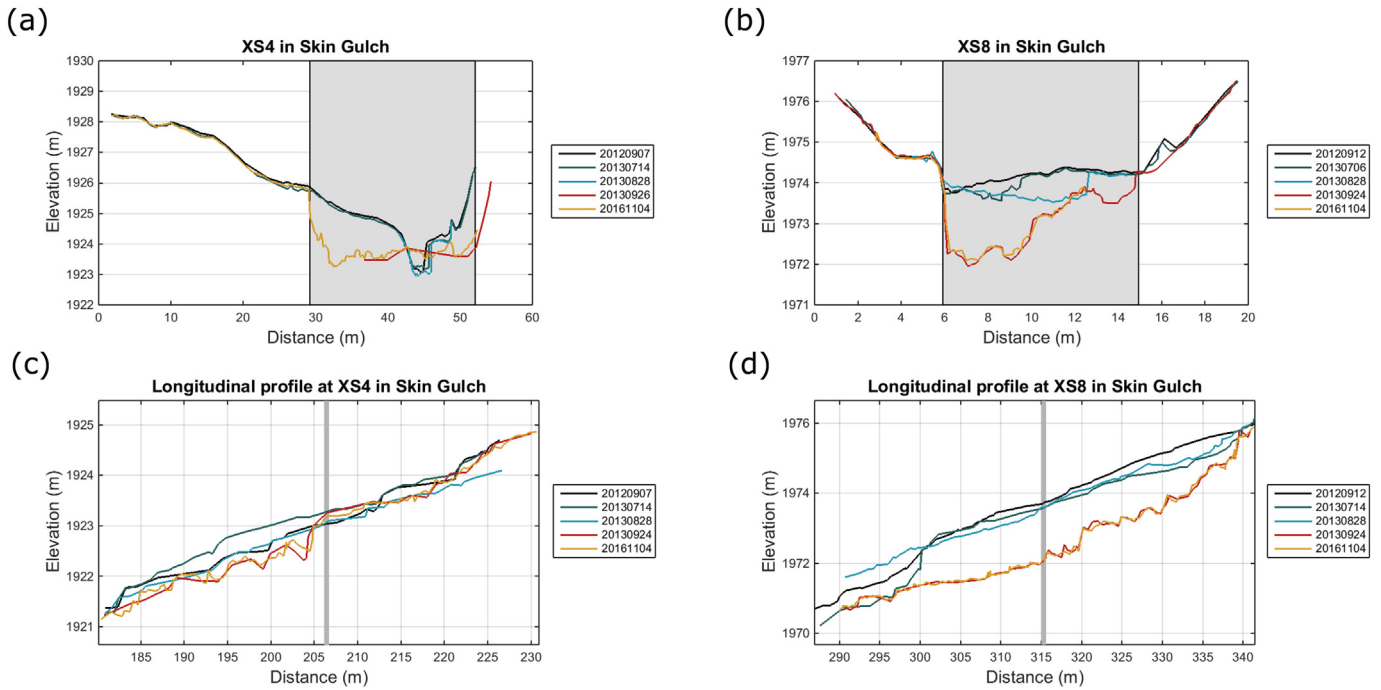
Fig. 2. Changes over time for cross-sections (a) XS4 and (c) XS8 in Skin Gulch, and (b, d) the corresponding longitudinal profiles. The gray shaded box in (a) delineates the active channel and the vertical line in (b) and (d) shows the location of the cross section. The three surveys in the black to blue colors were selected to emphasize the relatively large magnitude of XS changes prior to the mesoscale flood, and the two surveys in red and orange show both the large magnitude of change due to the mesoscale flood and the much smaller magnitude of XS change following the mesoscale flood. (For interpretation of the references to color in this figure legend, the reader is referred to the web version of this article.)

been deposited after the HPF was eroded along with substantial amounts of the pre-existing floodplain deposits. In absolute terms, the stripping of deposited sediment generally increased channel cross-sectional areas and decreased thalweg elevations (e.g., Figs. 2, 3, 6, 7; Tables 2 and 3). The large amounts of channel erosion and scour in the modeled reaches resulted in considerable uncertainty in our

modeled peak flows depending on whether we used the pre- or post-flood topography. In SG, the estimated peak flow using pre-flood topography was 2.3 m^3 s^{-1} km^{-2} as compared to the much larger value of 5.7 m^3 s^{-1} km^{-2} using post-flood topography (Brogan et al., 2017). In HG, the corresponding estimates of the peak flows were 0.9 m^3 s^{-1} km^{-2} using pre-flood topography and about 50% larger or
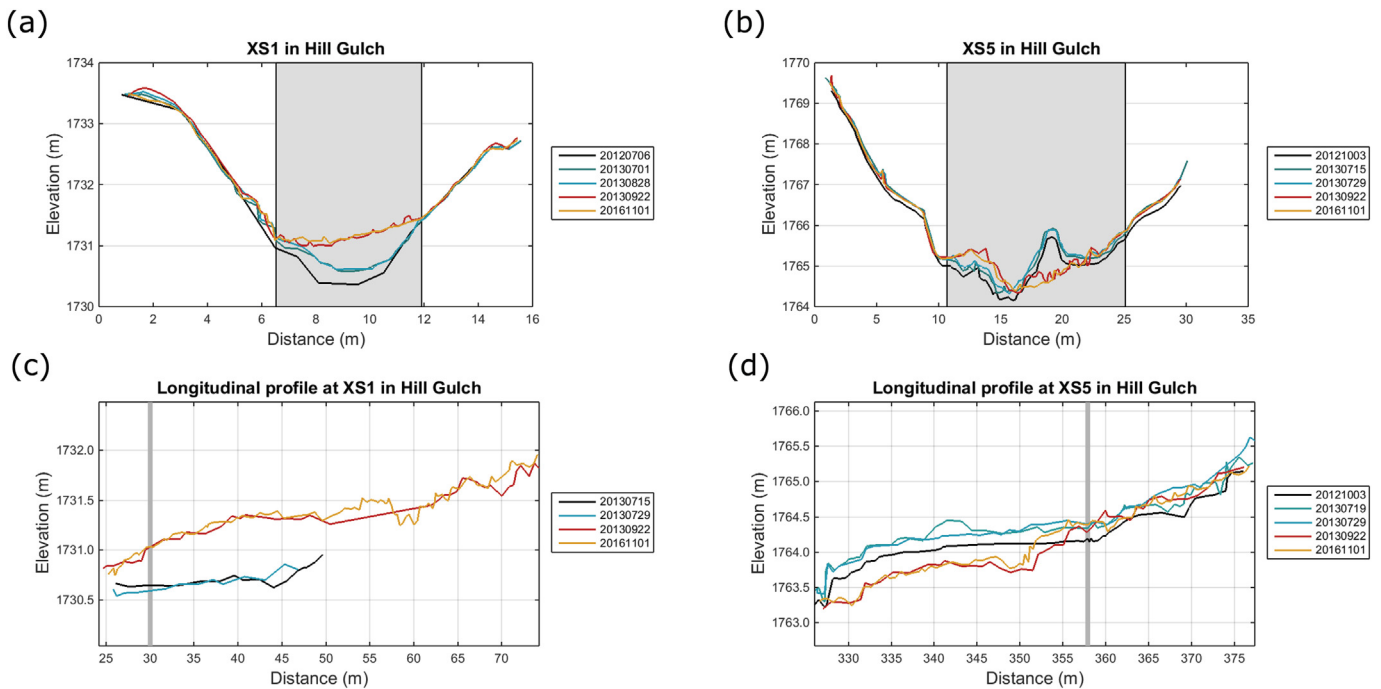
Fig. 3. Changes over time for cross-sections (a) XS1 and (c) XS5 in Hill Gulch, and (b, d) the corresponding longitudinal profiles. The gray shaded box in (a) delineates the active channel and the vertical line in (b) and (d) shows the location of the cross section. The three surveys in the black to blue colors were selected to emphasize the relatively large magnitude of XS changes prior to the mesoscale flood, and the two surveys in red and orange show both the large magnitude of change due to the mesoscale flood and the much smaller magnitude of XS change following the mesoscale flood. (For interpretation of the references to color in this figure legend, the reader is referred to the web version of this article.)
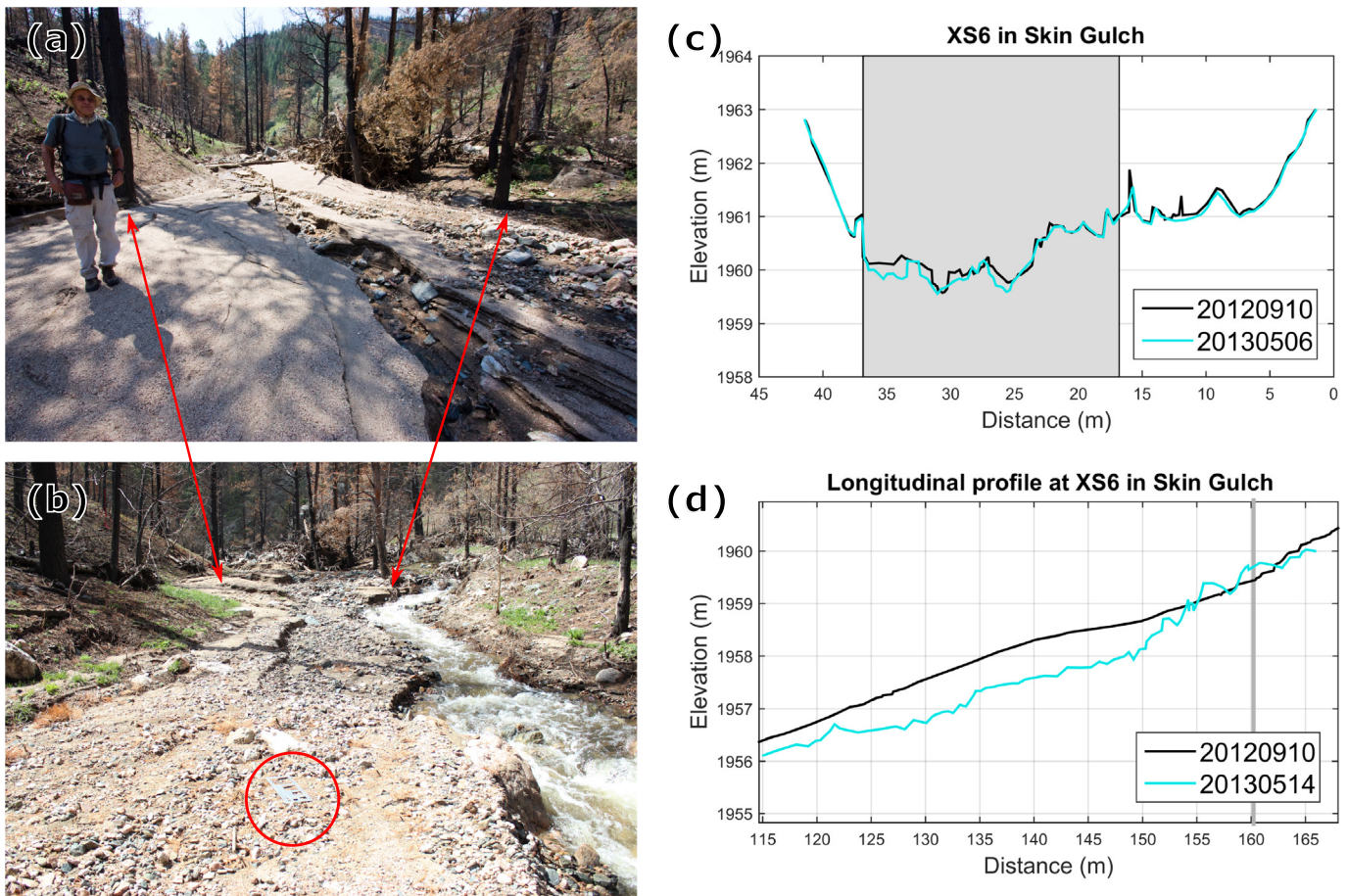
Fig. 4. (a) Photo looking upstream from below cross section six (XS6) in Skin Gulch on 8 March 2013 showing the extensive deposition from the summer thunderstorms. (b) Photo taken at the same location on 10 May 2013 showing the subsequent incision and floodplain coarsening during spring snowmelt; red circle indicates a gravelometer for scale. (c) Cross sections and (d) longitudinal profiles in fall 2012 (black line) and spring 2013 (blue line). Gray shaded box in (c) delineates the active channel and the vertical line in (d) represents the location of the cross section. XS6 is in the foreground of the photo in (a) and in the far background of the photo in (b), and in (c) XS6 is plotted looking upstream to match the perspective of the two photos. (For interpretation of the references to color in this figure legend, the reader is referred to the web version of this article.)

$1.4\,\mathrm{m^3\,s^{-1}\,km^{-2}}$ using post-flood topography. These data mean that the estimated peak flows in HG were only 25–39% of the estimated peak flows in SG.

Channel and valley bottom changes were far greater in SG than in HG, which is consistent with the 2.5- to 4-fold difference in the estimated peak flows. In SG, there was a general trend of incision in the upstream XSs where valley widths were narrower (e.g., Fig. 2b; see also Fig. 3 in Brogan et al., 2017), while channel widening was more predominant in the downstream XSs where the valleys were wider (e.g., Fig. 2a; Tables 1 and 2). In SG, the mean absolute change in cross-sectional area was $7.7\,\mathrm{m^2}$, and there was net erosion at every XS. The greatest absolute change in cross-sectional area was $18.2\,\mathrm{m^2}$ at XS5 (Fig. 6); this XS had large overbank sediment deposits from the 2012 convective flood and nearly all of that sediment was eroded away by the 2013 flood. The mean bed elevation change for the XSs in SG was a decrease of 0.37 m, and the mean thalweg incision was 0.67 m (Table 2). The greatest incision of nearly 1.6 m occurred at XS8 (Fig. 2b), which is the cross section with the narrowest valley width of just 13 m (Table 1).

In HG, the mean absolute change in cross-sectional area due to the mesoscale flood was only $1.3\,\mathrm{m^2}$, or just 17% of the corresponding mean change in SG. There was not the same trend of channel incision in the upstream XSs and channel widening in the downstream XSs (Table 3) as in SG, and this may be due to the lack of a consistent downstream increase in valley widths (Table 1). The upper eight XSs all incised, but their mean elevation change was only −0.07 m or 18% of the mean elevation change for XS2–XS10 in SG (Table 3). In the three lowest XSs in HG, there was net deposition, with the greatest mean

aggradation being 0.32 m in XS1 (Table 3; Fig. 3a, c). The much greater deposition inXS1 is consistent with its much lower slope of 1.1% as compared to the 5% slope at XS2 and nearly 4% slope at XS3 (Table 3).

Channel incision and widening during the mesoscale flood also led to knickpoint migration and local slope changes, especially in SG. For the nine XSs in SG with valid post-flood data, the mean absolute change in slope was 1.2% with a maximum increase of 2.4% at XS2 (Table 2). A closer review shows that within a LP there tended to be a greater increase in slope and greater incision where there had been more deposition (Fig. 2c, d). However, incision was limited by bedrock in six of the nine LPs in SG. In HG, the mean absolute change in LP slope was only 0.5%, or less than half of the mean change in SG, even though bedrock limited incision in only three of the eleven LPs (Fig. 7; Table 3). Since the slope changes tended to be greater in the LPs with more deposition, the smaller mean slope change in HG can be explained by the smaller amounts of post-fire deposition. In both watersheds there was more incision in the steeper LPs (Tables 2 and 3), with LP slope explaining just over 50% of the mean change in LP elevations. The larger incision in areas with steeper slopes is presumably because these reaches were more confined and had less opportunity for channel widening compared to the lower-gradient and less confined reaches further downstream.

The sustained flows of the mesoscale flood also caused substantial coarsening of the channel bed at all of the XSs (Fig. 5). In SG, the mean D_{84} nearly doubled from 68 mm to 126 mm, and in HG the mean D_{84} also nearly doubled from 60 mm to 110 mm (Fig. 5). The absolute variability in the D_{84} among XSs also decreased in both watersheds despite
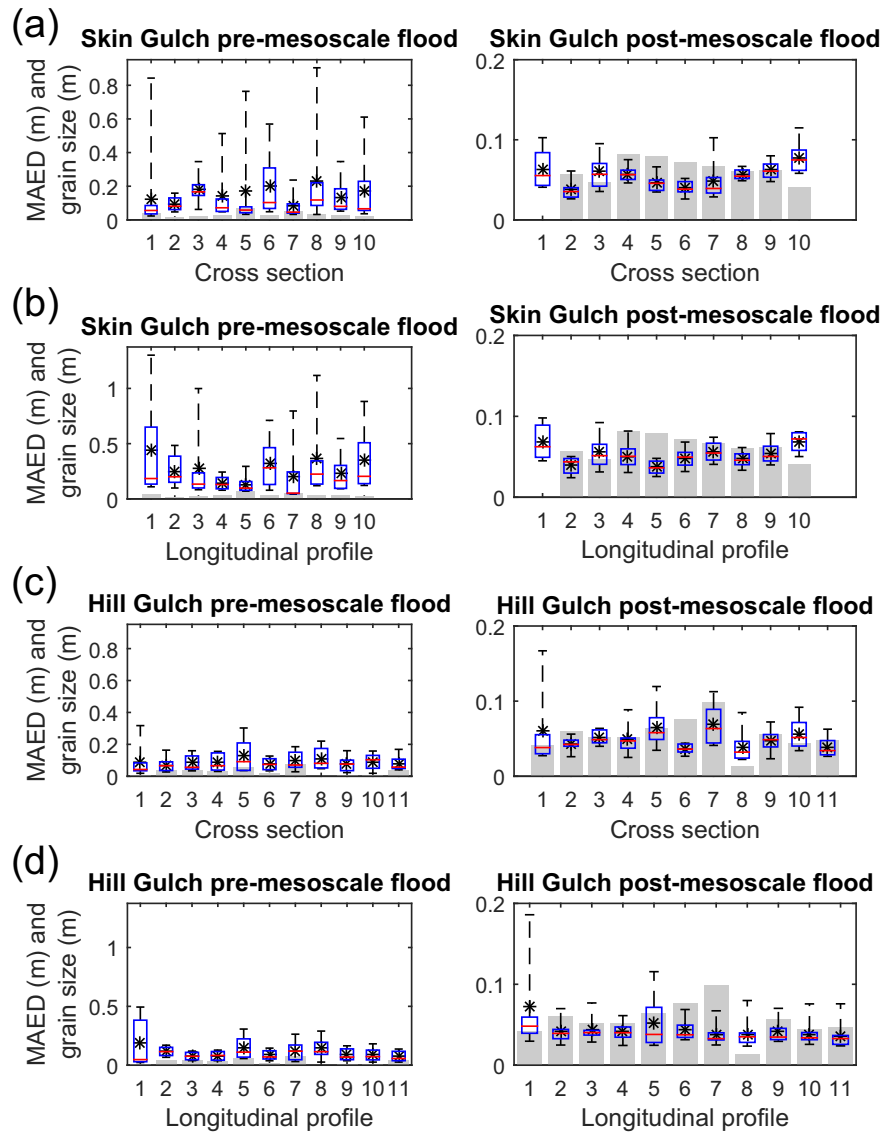
Fig. 5. Boxplots of the mean absolute elevation differences (MAED) for the different surveys prior to (left side) and after the mesoscale flood (right side) for the cross sections (a, c) and longitudinal profiles (b, d) in Skin Gulch and Hill Gulch, respectively. Boxes represent the 25th and 75th percentiles, red line is the median, mean is indicated by an *, and the whiskers show the minimum and maximum values. The gray bars show the D_{84} grain size divided by two for the pebble counts just prior to and shortly after the mesoscale flood, and the radius instead of the diameter is used as this helps indicates the potential uncertainty in the measured elevations due to the exact placement of the survey rod. No particle-size data are available for XS1 in SG after the mesoscale flood because of the sediment removal and channel reconstruction. Median MAED results are provided in Table 2 and Table 3. (For interpretation of the references to color in this figure legend, the reader is referred to the web version of this article.)

the large increase in the D_{84} (Fig. 5). The mean D_{16} increased from 3.8 to 7.0 mm in SG and 2.8 to 8.0 mm in HG, indicating that the finer particles were being winnowed out and transported down into the Cache la Poudre River.
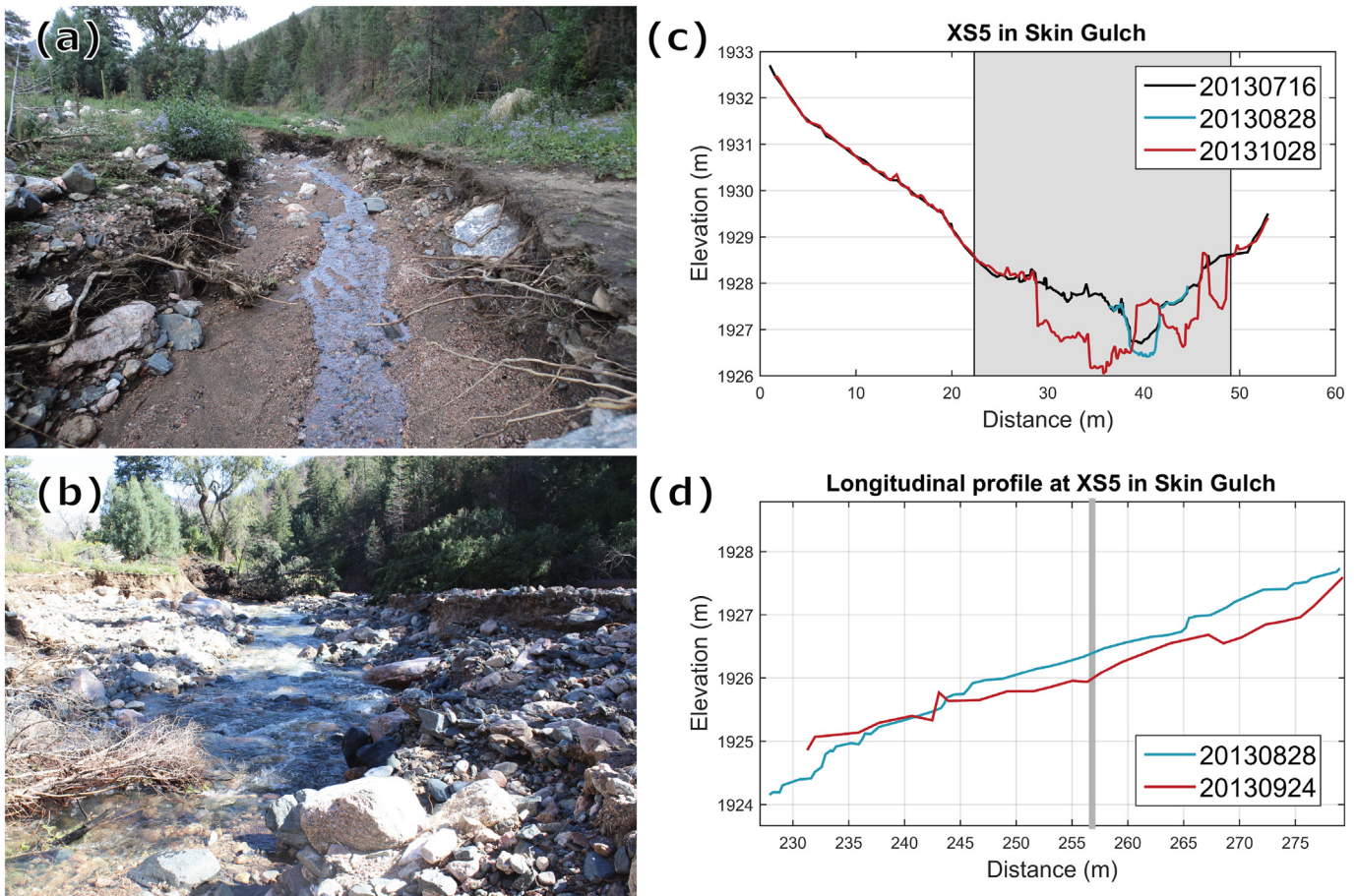
4.3. Post-mesoscale flood

Over the post-flood period from fall 2013 through summer 2016, there were much smaller and less frequent elevation changes in the channel XSs and LPs than in the first 15 months after burning (Figs. 2, 3, and 5; Tables 2 and 3). For the post-flood period, the median MAED values for all XS and LP changes were typically only about 5 cm (Tables 2 and 3), and in both watersheds the median post-flood MAED values were about 50% lower than the pre-flood values. Out of the 21 XSs and LPs, there were only two XSs (SG XS1 and 10) and two LPs (SG LP7 and HG LP1) where the elevation changes for the post-flood period were marginally larger than the elevation changes in the pre-flood period (Tables 2 and 3).

The small elevation changes in the XSs and LPs are especially note-worthy since our field observations indicated that highest spring runoff over the entire monitoring period occurred in the spring after the meso-scale flood. In summer 2014 we recorded virtually no deposition or ero-sion at any of our XSs or LPs (e.g., Figs. 2 and 3), and this is almost certainly due to the combination of increased vegetation cover and fewer high-intensity summer thunderstorms (Schmeer et al., 2018).

While there were slightly larger channel changes recorded in sum-mer 2015 than summer 2014, the absolute elevation changes in both the XSs and LPs were relatively minor. During the spring and summer of 2016 there were virtually no channel changes from either spring snowmelt or summer thunderstorms, indicating a cessation of signifi-cant post-fire and post-flood channel response.

4.4. Historic 1976 Flood

The July 1976 flood in the Big Thompson River just to the south of our study watersheds was notorious for killing 144 people and

Fig. 6. Photos looking downstream at cross section five (XS5) in Skin Gulch on (a) 28 August 2013 and (b) 24 September 2013 showing the channel erosion and coarsening caused by the mesoscale flood. Plots of the (c) cross section and (d) longitudinal profile prior to (blue line) and just after the mesoscale flood (red line). The 16 July 2013 XS (black line) is also shown in (c) because the XS survey on 28 August 2013 was limited to the main channel. Gray shaded box in (a) delineates the active channel and the vertical line in (b) represents the location of the cross section. (For interpretation of the references to color in this figure legend, the reader is referred to the web version of this article.)

destroying Colorado Highway 36 (McCain and Shroba, 1979). The estimated rainfall at the center of the storm was a little over 300 mm in just over 4 h.

This same storm also spilled over into parts of the Cache la Poudre watershed (McCain and Shroba, 1979), and total rainfall in HG was estimated at 240 to nearly 300 mm as compared to 200–240 mm in SG (Brogan, 2018). Aerial imagery taken two months after the flood shows that a historic dirt road and the valley bottom in the lower portion of SG (XS2 to XS6) experienced no dramatic flood-induced changes (see Fig. 3.16 in Brogan, 2018). In contrast, this same road was cut numerous times as a result of the large thunderstorm-driven flood in early July 2012, and then largely obliterated during the September 2013 mesoscale flood.

In HG, the 1976 flood caused much larger geomorphic changes as the high flow in the lower portion of HG eroded much of the valley bottom and mobilized large boulders (Fig. 8). A long-time resident in the lower portion of HG provided photographs showing how the flood eroded into the floodplain, causing a 1.8-m raw vertical bank near his house, leaving a very wide, coarse-textured channel (H.A. Fonken, pers. comm., 2017). Mr. Fonken also recounted that the dirt road up to his house from Highway 14 was completely washed out, and that "there were a lot more cobbles and boulders exposed…boulders five and six feet [1.5–1.7 m] high in diameter" (Fig. 8a). He also reported that the tributary just below XS2 deepened 2 or 3 ft [0.6–0.9 m] due to the 1976 flood, and during the 2013 mesoscale flood, this incised down to a similar level. These observations suggest that the mesoscale flood removed much of the sediment that had accumulated in lower HG over the 37 years between the 1976 and 2013 floods. The historic

accounts of the 1976 flood and our monitoring results document the far greater channel and valley bottom changes in lower HG from the 1976 flood than from the 2013 flood, even though the two storms had similar amounts of total precipitation (Fig. 8; see additional paired photos in Figs. C.28–C.31 in Brogan, 2018). This difference can be attributed to the much shorter duration of the rainfall for the 1976 flood, which would have generated much higher peak flows relative to our estimates for the 2013 mesoscale flood. Mr. Fonken also noted that Hill Gulch and Falls Gulch (a smaller watershed just to the west of HG) were the only two tributaries to the Cache la Poudre River that were greatly altered by the 1976 flood, corroborating our assessment that lower SG was not substantially altered by the rainstorm that caused the 1976 Big Thompson flood.

5. Discussion

5.1. Complex response after wildfire and its truncation by the mesoscale flood

Prior to the mesoscale flood, the channels in Skin Gulch and Hill Gulch exhibited a complex post-fire response (cf. Laird and Harvey, 1986; Moody and Martin, 2001). Convective thunderstorms delivered temporally short-term and spatially varying amounts of runoff and sediment from the hillslopes and upstream tributaries to the main channels and valley bottoms. The relative balance between deposition and transport depended primarily on the amounts of runoff and eroded sediment along with sediment particle size and density. In general, the ash, silt, and clay fractions were transported out of our study watersheds to the
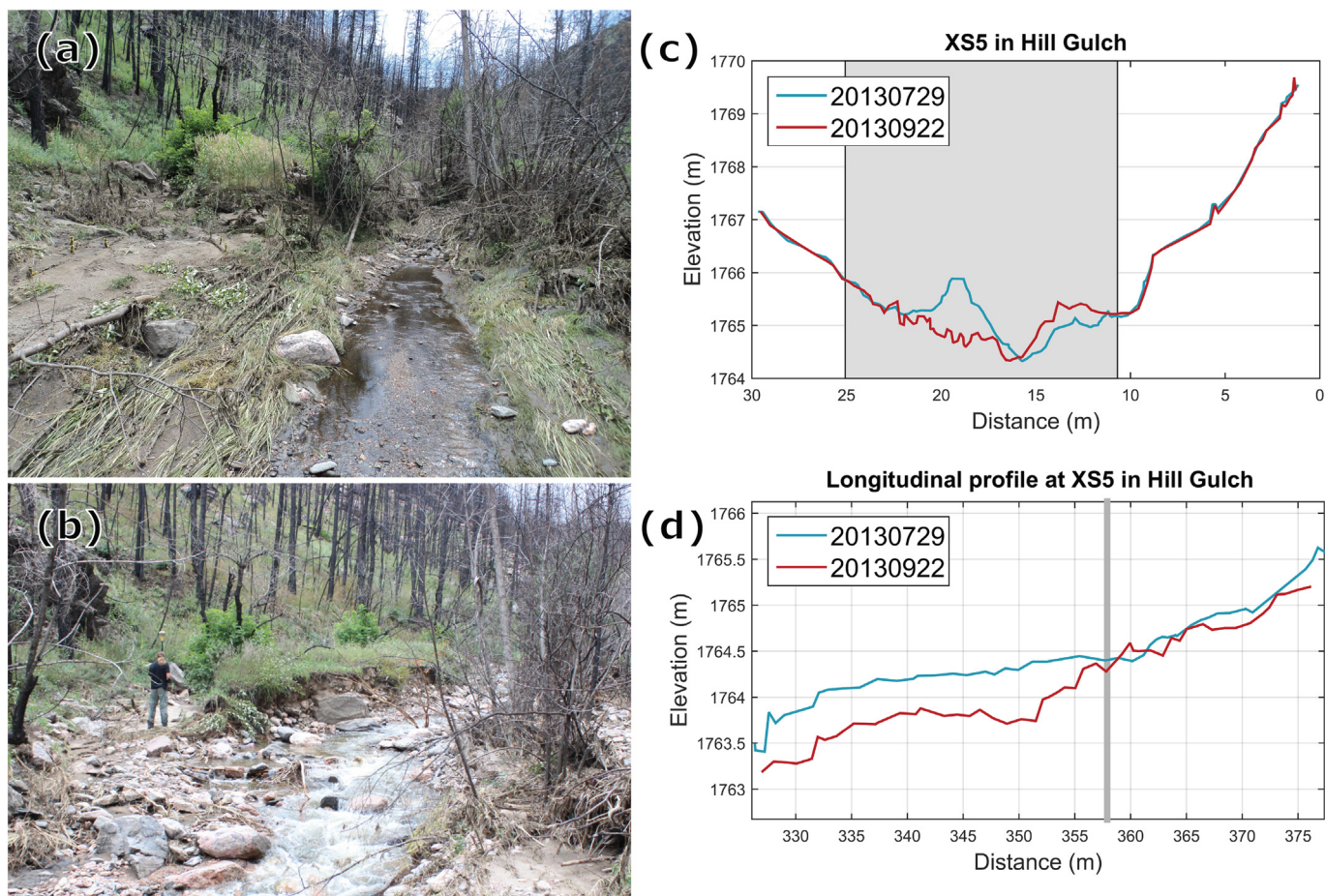
Fig. 7. Photos looking upstream at cross section five (XS5) in Hill Gulch on (a) 1 August 2013 and (b) 22 September 2013 showing the more moderate erosion in HG due to the mesoscale flood; a person in (b) provides scale. (c) Cross sections and (d) longitudinal profiles prior to (blue line) and just after the mesoscale flood (red line). The cross section is plotted looking upstream to match the perspective in the photos. The cross section in (c) is approximately where the person is standing in (b). (For interpretation of the references to color in this figure legend, the reader is referred to the web version of this article.)

Cache la Poudre River as evidenced by the very high turbidities in the thunderstorm runoff and the initial snowmelt pulse in spring 2013 (Hohner et al., 2016; Writer et al., 2014), our measured D_{16} values, and our qualitative observations of the post-fire sediment deposits.

There also were complex spatial variations in the balance between deposition and erosion in the valley bottoms. Some of the lower-lying deposits closer to the channel margin, especially the finer gravel and sand, were eroded and reworked by the runoff from subsequent thunderstorms, while the higher deposits remained largely undisturbed. The more intense thunderstorms, particularly in the first summer after burning, often generated sufficient hillslope erosion to cause downstream deposition rather than eroding older deposits. In contrast, and similar to other studies, spring snowmelt invariably eroded some of the recent post-fire deposits (e.g., Reneau et al., 2007) and in some cases cut down into the underlying pre-fire deposits. In the second summer after burning the higher-intensity thunderstorms again generated infiltration-excess overland flow and hillslope erosion, with much of this sediment being deposited in the valley bottoms, while the runoff from lower-intensity rainstorms and the higher baseflows induced by the vegetation loss caused channel incision and downstream transport of the finer particles. This same pattern, where higher intensity storms resulted in net aggradation while lower intensity storms resulted in net erosion, was noted in two ephemeral watersheds about 10 km west of SG (Rathburn et al., 2017).

These processes and overall patterns of erosion and deposition were similar between the two study watersheds, but the magnitude of channel changes was much greater in SG than in HG. This difference can be attributed in large part to the tremendous amount of sediment that was deposited as a result of the very high-intensity thunderstorm and large flood in the western part of SG just one week after the HPF was contained (Brogan et al., 2017). The largest and coarsest deposits resulting from this flood were near XS6, as this XS is just below a major confluence where the steep, more confined western tributary empties into a much wider and lower gradient valley bottom. Hence, the post-fire response was not only complex over time, but also over space given the large spatial variations in rainfall, erosion, and deposition within and between the two watersheds in the first 15 months after burning. The importance of topographic controls on post-fire channel changes suggests that a geomorphic characterization of the channels and valley bottoms can help predict the spatial and temporal patterns of sediment storage, erosion, and delivery (e.g., Fuller, 2008; Surian et al., 2016; Wolman and Eiler, 1958; Yochum et al., 2017).

Our data suggest that the shifting complex response between erosion and aggradation depends on several factors, including spatial scale (i.e., hillslope, subwatershed, watershed), time since burning, storm rainfall, and changes in snowmelt and baseflows (e.g., Brogan, 2018; Laird and Harvey, 1986). For most fires, one would expect a relatively rapid decline in the size of peak flows as the hillslopes revegetate, and hence a persistence of the sediment deposited in the channels and valley bottoms. Data from nearby fires clearly show that hillslope erosion rates and presumably surface runoff drop to relatively low levels by about the third or fourth summers after burning (Benavides-Solorio and MacDonald, 2005; Larsen et al., 2009; Wagenbrenner et al., 2006), and hence a reduced potential for downstream channel

Fig. 8. Photos looking upstream from below cross section two (XS2) in Hill Gulch contrasting the effect of the (a) 1976 flood and the (b) 2013 mesoscale flood. The house in (a) burned in the 2012 High Park fire and the access road in (b) is not visible in (a) as it was completely washed away by the 1976 flood.

geomorphic change. In the High Park Fire, this expected timescale of recovery was confirmed by the decline in measured erosion rates for 29 convergent hillslopes in SG and HG, except for one large, localized thunderstorm in HG in August 2015 (Schmeer et al., 2018). This decline in hillslope runoff and erosion causes a corresponding reduction in downstream flooding, deposition, and sediment transport (e.g., Moody and Martin, 2001; Morris and Moses, 1987), and these processes—along with riparian vegetation regrowth—lead to a stabilization of the downstream channels.

In our case, the expected post-fire trajectory of primarily deposition with rapid vegetative colonization of the post-fire sediment deposits was suddenly truncated by the multiday September 2013 rainstorm. The sustained high flows resulting from this storm stripped away nearly all of the deposited post-fire sediment and reworked much of the pre-fire sediment in the floodplains and lower terraces. In some cases, such as the Buffalo Creek and Hayman fires in Colorado, the very coarse-textured granitic soils and associated poor growing conditions result in slower hillslope and channel recovery; the continued inputs of water and sediment to the channel network results in further cycles of deposition and erosion (Moody, 2017), slowing the vegetative recovery of the valley bottoms. In our two watersheds, the evacuation of nearly all of the post-fire sediment deposits by the mesoscale flood effectively reset the downstream channel system by creating much wider, coarser, and more deeply incised channels. The channel incision and coarsening of the substrate in the channels and valley bottoms is expected to slow the rate of vegetative regrowth, particularly in SG.

This evacuation of the post-fire sediment deposits and associated coarsening of the channel bed by the mesoscale flood may slow vegetative recovery, but it has greatly reduced the sensitivity, or increased the threshold, of the channels to future geomorphic change (e.g., Hooke, 2015; Schumm, 1979). This reduced sensitivity is evidenced by the very limited changes in the cross sections and longitudinal profiles after the mesoscale flood, despite the exceptionally high spring flows in 2014 and May 2015 when there were two large, rapidly melting snowstorms. The implication is that if the mesoscale flood had not occurred, the threshold for channel changes would have been lower as many of the finer-textured post-fire sediment deposits would have remained and been susceptible to channel and floodplain erosion. Hence, our study provides a unique example of how a mesoscale flood not only altered the expected trajectory of post-fire channel conditions, but also allows a direct comparison of the post-fire channel changes to the effects of an exceptional long-duration flood.

5.2. Differences in mesoscale flood response

Channel geomorphic changes from the 2013 mesoscale flood were far greater in SG than in HG, despite the similarity of these two watersheds in size, hypsometry, drainage density, slope, pre-fire vegetation, and areas subjected to different burn severities. Additionally, the depth and intensity of rainfall during the mesoscale storm were very similar in each watershed. We suggest three main reasons for the different response to the mesoscale flood between the two watersheds.

First, our hydrodynamic modeling indicated that the estimated peak flow for the mesoscale flood was 2.5 to 4 times larger in SG than HG. Our best estimate of the total energy available for geomorphic work, calculated by integrating the time series of stream power for the minimum and maximum channel dimensions, was 30,000–50,000 kJ in SG (Brogan et al., 2017) as compared to only 11,000–16,000 kJ in HG. This difference results in a much lower sediment transport capacity (e.g., Julien, 2010) and energy available for geomorphic work in HG (e.g., Costa and O'Connor, 1995), which can then help explain the much greater channel incision and widening in SG compared to HG. We posit that some of the difference in peak flows and total energy expended between SG and HG may be due to the spatial differences in burn severity as the total amount and intensity of the rainfall for the mesoscale storm was relatively similar between the two watersheds (Kampf et al., 2016). Areas burned at high and moderate severity generate much more and faster runoff than areas burned at low severity due to the large decreases in rainfall interception, infiltration rates and surface roughness, and the resulting large increase in channel density and hillslope-channel connectivity (e.g., Moody et al., 2008). In SG, the areas burned at high and moderate severity were mostly in the upper part of the watershed, while in HG, the majority of areas burned at high and moderate severity were in the lower part of the watershed. The rainfall data shows that during the mesoscale storm, there were two distinct, high-intensity bursts of rainfall that caused the largest peak flows. The higher burn severities in the upper portion of SG would have resulted in more rapid runoff and a shorter time to concentration that could have synchronized runoff from the upper parts of the watershed with the smaller and slower peak flows from the lower portion of the watershed, increasing the absolute magnitude of the peak flow in the lower portion of SG (sensu Mejía and Moglen, 2010). In HG, there would be less and slower runoff from the less severely burned, upper portions of the watershed, while the stormflows from the lower, more severely burned portions of the watershed would have a relatively short time of concentration, resulting in a desynchronization of the runoff peaks compared to SG.

The legacy of the 1976 flood may be a second important reason for the greater geomorphic response to the mesoscale flood in SG than HG. Photos and our interview with a landowner indicate that in HG the 1976 flood removed much of the valley fill and coarsened the channel in lower HG, and the effect of this flood is still clearly evident from

hillslope and floodplain escarpments, and large depositional bars composed of cobbles and boulders. The geomorphic effects of the 1976 flood are remarkably similar to the changes observed in SG as a result of the 2013 mesoscale flood (e.g., compare Figs. 6b and 8a). Since erosion rates in the Colorado Front Range are only about 20–60 mm/k.a. (e.g., Dethier et al., 2014; Foster et al., 2015), only a relatively small amount of hillslope erosion and downstream sediment deposition would have occurred between the 1976 flood and the HPF in 2012. After the HPF, the summer thunderstorms in 2012 and 2013 did increase the amount of sediment stored in the channels and valley bottoms in HG, but the magnitude of post-fire sediment deposits was much less than in SG. Hence, the channels and valley bottoms in lower HG had a lower sensitivity to, and less potential for, geomorphic change than the channels and valley bottoms in SG (e.g., Costa and O'Connor, 1995; Hooke, 2015; Schumm, 1979).

A third reason for the very large response in SG to the 2013 mesoscale flood is that SG had such large post-fire sediment deposits in the channel and valley bottoms, particularly from the high-intensity thunderstorm in July 2012 (Brogan et al., 2017). The large volumes of post-fire sediment in and adjacent to the stream channels in the lower portion of the watershed effectively 'loaded the gun' (sensu Nanson, 1986) by increasing the amount of sediment that could be eroded by subsequent high flows. Our data and field observations show that the vast majority of this post-fire sediment, along with some of the older floodplain and valley bottom deposits, were removed during the 2013 mesoscale flood. In contrast, there was much less pre- and post-fire sediment in HG, resulting in less net channel change. It follows that if the 2012 flood in SG had not happened, the effects of the 2013 flood in SG would not have been as dramatic. The unusual flood-fire-flood sequence that we were able to document shows how the effect of a given disturbance can vary according to the pre-existing sequence of events. The implication is that predicting the geomorphic effects of large floods requires an assessment and understanding of the legacy effects from past fires and other disturbances, as this can greatly alter the relative sensitivity to a subsequent external forcing (e.g., Germanoski, 2002; Hooke, 2015; Wolman and Gerson, 1978). Our ability to understand and predict post-fire erosion and deposition at the watershed scale could greatly improve with additional research from watersheds with varying disturbance histories.

5.3. Comparing fire and flood effects

Direct comparisons of the geomorphic impacts of fires and floods are complicated by the choice of spatial and temporal scales, variability in rainfall amounts and intensities, multiple interacting processes associated with each kind of disturbance, and the varying persistence of different effects over space (Brunsden and Thornes, 1979; Moody et al., 2013). Anecdotal evidence (e.g., aerial photos and the lack of any historical accounts of large floods) suggests that prior to 1976 the downstream valleys in both SG and HG would have had a similar sensitivity to geomorphic change and were on a similar trajectory of slowly increasing sensitivity as sediment accumulated in the downstream valley bottoms (Fig. 9). In HG, the 1976 flood removed much of the accumulated sediment in the lowest portion of the watershed, greatly reducing the sensitivity of the downstream channels to subsequent disturbances and the potential for future geomorphic changes (Fig. 9).

As discussed above and shown in Fig. 9, there would have been a small increase in sensitivity in HG over the 36 years between the 1976 flood and the 2012 HPF as sediment accumulated in the lower watershed. The HPF induced extensive hillslope erosion and downstream deposition in both watersheds, with substantially more deposition in SG and a corresponding larger increase in sensitivity as shown in Fig. 9. In both watersheds, the September 2013 mesoscale flood stripped much of the sediment from the channels and adjacent valley bottoms, creating a similar insensitive condition in lower SG as in lower HG following the 1976 flood (e.g., compare Figs. 6b and 8a). Yet SG had burned, which led to very extensive downstream deposition prior to the mesoscale flood,
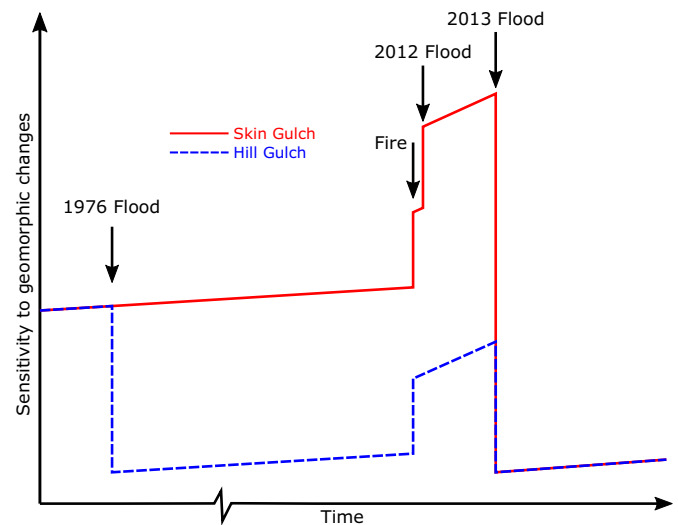
Fig. 9. Relative sensitivity over time of the channels and valley bottoms to geomorphic form change in Skin Gulch (red line) and Hill Gulch (dashed blue line). The step changes in sensitivity are respectively attributed to the 1976 flood in Hill Gulch, the 2012 High Park Fire, the 2012 convective flood in Skin Gulch, and the 2013 mesoscale flood. (For interpretation of the references to color in this figure legend, the reader is referred to the web version of this article.)

while HG was unburned prior to the 1976 flood. Thus, the two study watersheds took two very different pathways to a comparable state of relative insensitivity. If SG had not first burned and the convective flood had not caused the large amounts of deposition in the lower valley bottoms, the magnitude of erosion from the 2013 mesoscale flood would almost certainly have been much less. It is interesting to speculate what the lower portion of SG would have looked like after the 2013 mesoscale flood if it had not burned, and we hypothesize that channel erosion would not have been nearly as severe due to the lower rainfall intensities during the 2013 mesoscale flood compared to the much higher rainfall intensities in HG in 1976. Hence, the different pathways ultimately did affect the relative magnitude of geomorphic changes from the mesoscale flood, with HG having a much more muted response than SG and the much larger change in SG being at least partially due to its increased sensitivity following the HPF (Fig. 9).

Resilience has been defined as the ability of a system to absorb a perturbation without changing to a new state (Tabacchi et al., 2009), and it can be quantified by how fast a system recovers back to its initial state (Holling, 1996). In our study, we define sediment recovery in terms of the erosion and deposition in the valley bottoms causing changes in geomorphic form (i.e., valley fill). Given the relatively short 37-year window between the extreme floods of 1976 and 2013, the valley form in HG had not recovered by the time of the mesoscale flood, even with the additional sediment deposited following the HPF. By eroding nearly all of the post-fire sediment, the 2013 flood reduced the relative sensitivity of HG to a condition that is similar to SG and roughly comparable to the valley fill present after the 1976 flood. Looking forward, climate change will increase the frequency of extreme rainstorms (e.g., Berg et al., 2013), which will both increase the rate at which the valley bottoms will accumulate sediment and increase the risk of major floods that would again excavate the accumulated sediment. Climate change will also increase the frequency and severity of large fires, so there is a clear need to understand how different disturbance histories will affect the magnitude of future downstream erosion and sedimentation. This understanding then has important implications for safeguarding downstream landowners, water users, and aquatic biota.

The choice of spatial scale also is important for assessing the effect of forest fires on geomorphic sensitivity and resilience. In the ponderosa pine forests of the Colorado Front Range, the mean fire interval is about 10–50 years (Kaufmann et al., 2000; Veblen et al., 2000), yet the

hillslope-scale post-fire increases of runoff, erosion, and channel extension only last a few years (e.g., Benavides-Solorio and MacDonald, 2005; Larsen et al., 2009; Moody and Martin, 2001; Morris and Moses, 1987; Wohl and Scott, 2017). Consequently, the effects of fires on sediment fluxes at both the hillslope and watershed scale are relatively short-lived, at least in the Colorado Front Range where most of the post-fire erosion is driven by concentrated runoff rather than debris flows. It also can be argued that the effects of fires on geomorphic form also are relatively short-lived at the hillslope scale as colluvial processes tend to fill in the newly-formed drainage channels. At larger spatial scales, post-fire hillslope and headwater erosion can result in substantial downstream deposition as shown here and in other studies (e.g., Meyer et al., 1992; Moody and Martin, 2001; Reneau et al., 2007). In the Colorado Front Range, the recurrence interval (RI) for these larger-scale fire-flood sequences have been estimated at hundreds to thousands of years (e.g., Cotrufo et al., 2016; Elliott and Parker, 2001), resulting in much longer-term form changes as compared to the much shorter-term changes in sediment flux.

The September 2013 mesoscale flood had a RI on the order of tens to hundreds of years (Yochum, 2015), and like the 1976 flood in HG it stripped away valley bottom deposits in both burned and unburned watersheds (e.g., Gartner et al., 2015; Wicherski et al., 2017; Yochum et al., 2017). Given the low long-term erosion rates in the Colorado Front Range, it could take hundreds of years for the valleys to refill and return to their predisturbance form. The implication is that form recovery in channels and valley bottoms may take longer after extreme floods than after wildfires (e.g., Rathburn et al., 2017).

Several process-based arguments provide additional support for the assertion that fires will have a more limited geomorphic effect at larger scales and a shorter form recovery period than extreme floods. First, the spatial extents of most fires are small, especially compared to the footprints of large floods. The area encompassed by the 2002 Hayman fire, which is still the largest fire in Colorado's recorded history, is 560 km^2, while the high rainfall area for both the 1976 Big Thompson flood and the 2013 mesoscale flood were at least a couple thousand square kilometers (e.g., Gochis et al., 2014; McCain and Shroba, 1979). Second, fires typically only burn parts of a large watershed and substantial proportions of the area within a fire perimeter are is either unburned or burned at low severity (this proportion was about 50% in the case of the HPF). The implication is that within any given watershed the post-fire effects will be significantly diluted by the much lower amounts of runoff and sediment from either unburned areas or areas burned at low severity. Third, the driving force for most post-fire erosion in this region is summer convective storms (e.g. Gary, 1975; MacDonald and Stednick, 2003; Moody and Martin, 2009) that typically cover only a small area, so convective storms generate substantial amounts of runoff and overland flow from only a relatively small portion of a large burned area. It also should be reiterated that the high intensity rainfall from summer convective storms typically lasts for less than an hour, limiting both the spatial extent and the duration of the resulting high flows. For larger-sale floods, like those in 1976 and 2013, the rain is falling on a relatively resilient or insensitive landscapes, but the storms last for at least several hours and the resulting large accumulations of runoff result in much larger and more sustained high flows than after fires. This results in more geomorphic work (e.g., Costa and O'Connor, 1995) and greater channel changes in larger watersheds than the dramatic but much more localized geomorphic effects observed after wildfires (e.g., Fig. 9). Hence, fires can be an important source of sediment for downstream reaches, but large floods can readily erode this sediment and are much more dominant than fires in terms of shaping larger-scale channels and valleys in much of the Rocky Mountains.

6. Conclusions

Geomorphic changes were quantified in the channels and valley bottoms in two ~15 km^2 watersheds after the 2012 High Park Fire and subsequent floods. Post-fire summer convective thunderstorms caused extensive overland flow and hillslope erosion that delivered and deposited sediment into the downstream channels, particularly in the Skin Gulch watershed. The enhanced post-fire baseflows and spring snowmelt incised through these deposits, and the thunderstorms in the second summer deposited additional sediment and also reworked some of the lower-lying post-fire deposits. These relatively typical post-fire channel responses were interrupted 15 months after the fire by a long-duration flood that stripped the valleys of nearly all of the post-fire sediment as well as causing extensive erosion of some of the older valley bottom deposits. The much greater channel incision, widening, and coarsening in Skin Gulch than Hill Gulch is attributed to: (1) the larger peak flow and correspondingly greater energy expenditure in SG stemming from the different spatial patterns of burn severity between the two watersheds; (2) the reduced sensitivity in Hill Gulch as a result of the severe channel and valley bottom erosion caused by an extreme flood in 1976; and (3) the increased sensitivity in Skin Gulch as a result of the post-fire deposition associated with the 2012 convective flood, which effectively loaded the gun for the subsequent erosion by the large mesoscale flood in September 2013.

The sequence of floods and fires in our study watersheds show that fires greatly increase runoff and erosion for a relatively short period, and the downstream delivery and deposition of this sediment increases their sensitivity to subsequent disturbances, such as large floods. However, the post-fire changes are progressively diminished at larger scales, and the downstream post-fire effects are much smaller than the tremendous channel erosion, widening, and coarsening that can occur as result of larger-scale rainstorms and sustained high flows. Hence, large floods in mountainous regions can have the opposite effect of fires in terms of eroding accumulated sediment and decreasing the sensitivity of the channels and valley bottoms to future disturbances. The pre-fire disturbance history can affect the sensitivity of a watershed to subsequent disturbances, and additional downstream monitoring is needed to assess the larger-scale and longer-term effects of fires in watersheds with different disturbance histories. We conclude that the timing and sequence of different disturbances are critical controls on the relative sensitivity of watersheds to downstream channel change, and that extreme floods in the central Rocky Mountains are more dominant at shaping downstream valleys than the effects of wildfires.

Appendix A. Supplementary material

Supplementary data to this article can be found online at https://doi.org/10.1016/j.geomorph.2019.03.031.

References

Abbott, J.T., 1970. Geology of Precambrian rocks and isotope geochemistry of shear zones in the Big Narrows area, northern Front Range, Colorado. US Geological Survey (Open-File Report OF-70-1).

Abbott, J.T., 1976. Geologic map of the Big Narrows quadrangle, Larimer County, Colorado. US Geological Survey, Geologic Quadrangle Map, GQ-1323.

Baker, V.R., 1977. Stream-channel response to floods, with examples from central Texas. Geol. Soc. Am. Bull. 88, 1057–1071. https://doi.org/10.1130/0016-7606(1977) 88<1057:SRTFWE>2.0.CO;2.

Baker, V., Costa, J., Baker, V., 1987. Flood power. In: Costa, J. (Ed.), Catastrophic Flooding. Allen and Unwin, pp. 1–21.

Benavides-Solorio, J., MacDonald, L.H., 2001. Post-fire runoff and erosion from simulated rainfall on small plots, Colorado Front Range. Hydrol. Process. 15, 2931–2952. https:// doi.org/10.1002/hyp.383.

Benavides-Solorio, J., MacDonald, L.H., 2005. Measurement and prediction of post-fire erosion at the hillslope scale, Colorado Front Range. International of Wildland Fire 14, 457–474. https://doi.org/10.1071/WF05042.

Berg, P., Moseley, C., Haerter, J.O., 2013. Strong increase in convective precipitation in response to higher temperatures. Nat. Geosci. 6, 181–185. https://doi.org/10.1038/ ngeo1731.

Braddock, W.A., Abbott, J.T., Connor, J.J., Swann, G.A., 1988. Geologic map of the Poudre Park quadrangle, Larimer County, Colorado. US Geological Survey, Geologic Quadrangle Map, GQ-1620.

Brierley, G.J., 2010. Landscape memory: the imprint of the past on contemporary landscape forms and processes. Area 42, 76–85. https://doi.org/10.1111/j.1475-4762.2009.00900.x.

Brogan, D.J., 2018. Spatial and temporal channel changes across the watershed scale following wildfire and floods. PhD dissertation. Department of Civil and Engineering, Colorado State University, Fort Collins, CO, p. 248.

Brogan, D.J., Nelson, P.A., MacDonald, L.H., 2017. Reconstructing extreme post-wildfire floods: a comparison of convective and mesoscale events. Earth Surf. Process. Landf. 42, 2505–2522. https://doi.org/10.1002/esp.4194.

Brunsden, D., Thornes, J., 1979. Landscape sensitivity and change. Trans. Inst. Br. Geogr. 4, 463–484. https://doi.org/10.2307/622210.

Cannon, S.H., Gartner, J.E., Rupert, M.G., Michael, J.A., Rea, A.H., Parrett, C., 2010. Predicting the probability and of postwildfire debris flows in the intermountain western United States. GSA Bull. 122, 127–144. https://doi.org/10.1130/B26459.1.

Collins, L.M., Ketcham, B., 2001. Fluvial geomorphic response of a northern California coastal stream to wildfire. In: Allen, S.G., Shook, W. (Eds.), Vision Fire - Lessons Learned from the 1995 fire. Point Reyes National Seashore, U.S. Department of the Interior, pp. 59–79.

Costa, J.E., O'Connor, J.E., 1995. Geomorphically effective floods. In: Costa, J.E., Miller, A.J., Potter, K.W., Wilcock, P.R. (Eds.), Natural and Anthropogenic Influences in Fluvial Geomorphology. American Geophysical Union, pp. 45–56.

Cotrufo, M.F., Boot, C.M., Kampf, S., Nelson, P.A., Brogan, D.J., Covino, T., Haddix, M.L., MacDonald, L.H., Rathburn, S., Ryan-Bukett, S., Schmeer, S., Hall, E., 2016. Redistribution of pyrogenic carbon from hillslopes to stream corridors following a large montane wildfire. Glob. Biogeochem. Cycles 30, 1348–1355. https://doi.org/10.1002/ 2016GB005467.

de Vente, J., Poesen, J., Arabkhedri, M., Verstraeten, G., 2007. The sediment delivery problem revisited. Prog. Phys. Geogr. 31, 155–178. https://doi.org/10.1177/ 0309133307076485.

DeBano, L.F., Neary, D.G., Ffolliott, P.F., 1998. Fire's effects on ecosystems. John Wiley & Sons.

Dethier, D.P., Ouimet, W., Bierman, P.R., Rood, D.H., Balco, G., 2014. Basins and bedrock: Spatial variation in 10Be erosion rates and increasing relief in the southern Rocky Mountains, USA. Geology 42, 167–170. https://doi.org/10.1130/G34922.1.

Doehring, D.O., 1968. The effect of fire on geomorphic processes in the San Gabriel Mountains, California. Rocky Mountain Geology 7, 43–65.

Ebel, B.A., Moody, J.A., Martin, D.A., 2012. Hydrologic conditions controlling runoff generation immediately after wildfire. Water Resour. Res. 48. https://doi.org/10.1029/ 2011WR011470.

Elliott, J.G., Parker, R.S., 2001. Developing a post-fire flood chronology and recurrence probability from alluvial stratigraphy in the Buffalo Creek watershed, Colorado, USA. Hydrol. Process. 15, 3039–3051. https://doi.org/10.1002/hyp.390.

Erskine, W., Saynor, M., 1996. Effects of catastrophic floods on sediment yields in southeastern Australia. In: Walling, D.E., Webb, B.W. (Eds.), Erosion and Sediment Yield: Global and Regional Perspectives: Proceedings of an International Symposium. IAHS, pp. 381–388.

Florsheim, J.L., Keller, E.A., Best, D.W., 1991. Fluvial sediment transport in response to moderate storm flows following chaparral wildfire, Ventura County, southern California. Geol. Soc. Am. Bull. 103, 504–511. https://doi.org/10.1130/0016-7606(1991) 103<0504:FSTIRT>2.3.CO;2.

Foster, M.A., Anderson, R.S., Wyshnytzky, C.E., Ouimet, W.B., Dethier, D.P., 2015. Hillslope lowering rates and mobile-regolith residence times from in situ and meteoric 10Be analysis, Boulder Creek Critical Zone Observatory, Colorado. GSA Bull. 127, 862–878. https://doi.org/10.1130/B31115.1.

Friedman, J.M., Lee, V.J., 2002. Extreme floods, channel change, and riparian forests along ephemeral streams. Ecol. Monogr. 72, 409–425. https://doi.org/10.2307/3100097.

Fryirs, K., 2013. (Dis)Connectivity in catchment sediment cascades: a fresh look at the sediment delivery problem. Earth Surf. Process. Landf. 38, 30–46. https://doi.org/ 10.1002/esp.3242.

Fryirs, K.A., 2017. River sensitivity: A lost foundation concept in fluvial geomorphology. Earth Surf. Process. Landf. 42, 55–70. https://doi.org/10.1002/esp.3940.

Fuller, I.C., 2008. Geomorphic impacts of a 100- flood: Kiwitea Stream, Manawatu catchment, New Zealand. Geomorphology 98, 84–95. https://doi.org/10.1016/j. geomorph.2007.02.026.

Gartner, J.D., Dade, W.B., Renshaw, C.E., Magilligan, F.J., Buraas, E.M., 2015. Gradients in stream power influence lateral and downstream sediment flux in floods. Geology 43, 983–986. https://doi.org/10.1130/G36969.1.

Gary, H.L., 1975. Watershed management problems and opportunities for the Colorado Front Range ponderosa pine zone: The status of our knowledge. US Department of Agriculture, Forest Service, Rocky Mountain Forest and Range Experiment Station. RM-RP-139 139, 32.

Germanoski, D., 2002. The importance of event sequencing on the geomorphic impact of wildfire in the central great basin. Geological Society of America Abstracts with Programs, p. 319.

Gochis, D., Schumacher, R., Friedrich, K., Doesken, N., Kelsch, M., Sun, J., Ikeda, K., Lindsey, D., Wood, A., Dolan, B., Matrosov, S., Newman, A., Mahoney, K., Rutledge, S., Johnson, R., Kucera, P., Kennedy, P., Sempere-Torres, D., Steiner, M., Roberts, R., Wilson, J., Yu, W., Chandrasekar, V., Rasmussen, R., Anderson, A., Brown, B., 2014. The great Colorado flood of September 2013. Bull. Am. Meteorol. Soc. 96, 1461–1487.

Hamilton, E., Horton, J., Rowe, P., Reimann, L., 1954. Fire-flood sequences on the San Dimas Experimental Forest. Forest Service - U.S. Department of Agriculture, California Forest and Range Experiment Station, Technical Paper No. 6.

Hohner, A.K., Cawley, K., Oropeza, J., Summers, R.S., Rosario-Ortiz, F.L., 2016. Drinking water treatment response following a Colorado wildfire. Water Res. 105, 187–198. https://doi.org/10.1016/j.watres.2016.08.034.

Holling, C.S., 1996. Engineering resilience versus ecological resilience. In: Schulze, P.C. (Ed.), Engineering within ecological constraints. National Academy Press, pp. 31–44.

Hooke, J., 2015. Variations in flood magnitude–effect relations and the implications for flood risk assessment and river management. Geomorphology 251, 91–107. https:// doi.org/10.1016/j.geomorph.2015.05.014.

Johansen, M.P., Hakonson, T.E., Breshears, D.D., 2001. Post-fire runoff and erosion from rainfall simulation: contrasting forests with shrublands and grasslands. Hydrol. Process. 15, 2953–2965. https://doi.org/10.1002/hyp.384.

Julien, P.Y., 2010. Erosion and Sedimentation. Cambridge University Press.

Kampf, S.K., Brogan, D.J., Schmeer, S., MacDonald, L.H., Nelson, P.A., 2016. How do geomorphic effects of rainfall vary with storm type and spatial scale in a post-fire landscape? Geomorphology 273, 39–51. https://doi.org/10.1016/j.geomorph.2016.08.001.

Kaufmann, M.R., Huckaby, L., Gleason, P., 2000. Ponderosa pine in the Colorado Front Range: Long historical fire and tree recruitment intervals and a case for landscape heterogeneity. In: Neuenschwander, L., Ryan, K. (Eds.), Proceedings of the Joint Fire Science Conference and Workshop: Crossing the millennium: integrating spatial technologies and ecological principles for a new age in fire management. University of Idaho, pp. 153–160.

Kochel, R.C., 1988. Geomorphic impact of large floods: review and new perspectives on magnitude and frequency. In: Baker, V.R., Kochel, R.C. (Eds.), Flood Geomorphology. John Wiley & Sons, pp. 169–187.

Krapesch, G., Hauer, C., Habersack, H., 2011. Scale orientated analysis of river width changes due to extreme flood hazards. Nat. Hazards Earth Syst. Sci. 11, 2137–2147. https://doi.org/10.5194/nhess-11-2137-2011.

Laird, J., Harvey, M., 1986. Complex-response of a chaparral drainage basin to fire. In: Hadley, R. (Ed.), Drainage Basin Sediment Delivery. International Association of Hydrological Sciences, Albuquerque, NM, pp. 165–183.

Larsen, I.J., MacDonald, L.H., Brown, E., Rough, D., Welsh, M.J., Pietraszek, J.H., Libohova, Z., de Dios Benavides-Solorio, J., Schaffrath, K., 2009. Causes of post-fire runoff and erosion: water repellency, cover, or soil sealing? Soil Science Society of America 73, 1393–1407. https://doi.org/10.2136/sssaj2007.0432.

Legleiter, C.J., Lawrence, R.L., Fonstad, M.A., Marcus, W.A., Aspinall, R., 2003. Fluvial response a decade after wildfire in the northern Yellowstone ecosystem: a spatially explicit analysis. Geomorphology 54, 119–136. https://doi.org/10.1016/S0169-555X (02)00332-X.

MacDonald, L.H., Stednick, J.D., 2003. Forests and water: A state-of-the-art review for Colorado. Colorado Water Resources Research Institute Completion Report.

Magilligan, F.J., Phillips, J.D., James, L.A., Gomez, B., 1998. Geomorphic and sedimentological controls on the effectiveness of an extreme flood. The Journal of Geology 106, 87–96. https://doi.org/10.1086/516009.

Magilligan, F.J., Buraas, E., Renshaw, C., 2015. The efficacy of stream power and flow duration on geomorphic responses to catastrophic flooding. Geomorphology 228, 175–188. https://doi.org/10.1016/j.geomorph.2014.08.016.

McCain, J.F., Shroba, R., 1979. Storm and Flood of July 31-August 1, 1976, in the Big Thompson River and Cache La Poudre River Basins, Larimer and Weld Counties, Colorado (Report number1115A,B).

Mejía, A.I., Moglen, G.E., 2010. Spatial distribution of imperviousness and the space-time variability of rainfall, runoff generation, and routing. Water Resour. Res. 46. https:// doi.org/10.1029/2009WR008568.

Meyer, G.A., Wells, S.G., Balling Jr., R.C., Jull, A.T., 1992. Response of alluvial systems to fire and climate change in Yellowstone National Park. Nature 357, 147–150. https://doi. org/10.1038/357147a0.

Meyer, G.A., Wells, S.G., Jull, A.J.T., 1995. Fire and alluvial chronology in Yellowstone National Park: Climatic and intrinsic controls on Holocene geomorphic processes. Geol. Soc. Am. Bull. 107, 1211–1230. https://doi.org/10.1130/0016-7606(1995) 107<1211:FAACIY>2.3.CO;2.

Miller, A.J., 1990. Fluvial response to debris associated with mass wasting during extreme floods. Geology 18, 599–602. https://doi.org/10.1130/0091-7613(1990)018<0599: FRTDAW>2.3.CO;2.

Montgomery, D.R., Buffington, J.M., 1997. Channel-reach morphology in mountain drainage basins. Geol. Soc. Am. Bull. 109, 596–611. https://doi.org/10.1130/0016-7606 (1997)109<0596:CRMIMD>2.3.CO;2.

Moody, J.A., 2016. Estimates of peak flood discharge for 21 sites in the Front Range in Colorado in response to extreme rainfall in September 2013. US Geol. Surv. Sci. Investig. Rep., 2016–5003 https://doi.org/10.3133/sir20165003.

Moody, J.A., 2017. Residence times and alluvial architecture of a sediment superslug in response to different flow regimes. Geomorphology 294, 40–57. https://doi.org/ 10.1016/j.geomorph.2017.04.012.

Moody, J.A., Martin, D.A., 2001. Initial hydrologic and geomorphic response following a wildfire in the Colorado Front Range. Earth Surf. Process. Landf. 26, 1049–1070. https://doi.org/10.1002/esp.253.

Moody, J.A., Martin, D.A., 2004. Wildfire impacts on reservoir sedimentation in the western United States. Proceedings of the Ninth International Symposium on River Sedimentation, pp. 1095–1102.

Moody, J.A., Martin, D.A., 2009. Synthesis of sediment yields after wildland fire in different rainfall regimes in the western United States. International of Wildland Fire 18, 96–115. https://doi.org/10.1071/WF07162.

Moody, J.A., Martin, D.A., Haire, S.L., Kinner, D.A., 2008. Linking runoff response to burn severity after a wildfire. Hydrol. Process. 22, 2063–2074. https://doi.org/10.1002/hyp.6806.

Moody, J.A., Shakesby, R.A., Robichaud, P.R., Cannon, S.H., Martin, D.A., 2013. Current research issues related to post-wildfire runoff and erosion processes. Earth Sci. Rev. 122, 10–37.

Morris, S.E., Moses, T.A., 1987. Forest fire and the natural soil erosion regime in the Colorado Front Range. Ann. Assoc. Am. Geogr. 77, 245–254. https://doi.org/10.1111/j.1467-8306.1987.tb00156.x.

Nanson, G.C., 1986. Episodes of vertical accretion and catastrophic stripping: a model of disequilibrium flood-plain development. Geol. Soc. Am. Bull. 97, 1467–1475. https://doi.org/10.1130/0016-7606(1986)97<1467:EOVAAC>2.0.CO;2.

Nelson, J.M., Shimizu, Y., Abe, T., Asahi, K., Gamou, M., Inoue, T., Iwasaki, T., Kakinuma, T., Kawamura, S., Kimura, I., et al., 2016. The International River Interface Cooperative: Public domain flow and morphodynamics software for education and applications. Adv. Water Resour. 93, 62–74. https://doi.org/10.1016/j.advwatres.2015.09.017.

Newson, M., 1980. The geomorphological effectiveness of floods–a contribution stimulated by two recent events in mid-Wales. Earth Surface Processes 5, 1–16. https://doi.org/10.1002/esp.3760050102.

Nuth, C., Kääb, A., 2011. Co-registration and bias corrections of satellite elevation data sets for quantifying glacier thickness change. Cryosphere 5, 271. https://doi.org/10.5194/tc-5-271-2011.

Onda, Y., Dietrich, W.E., er, F., 2008. Evolution of overland flow after a severe forest fire, Point Reyes, California. Catena 72, 13–20. https://doi.org/10.1016/j.catena.2007.02.003.

Poff, N.L., Allan, J.D., Bain, M.B., Karr, J.R., Prestegaard, K.L., Richter, B.D., Sparks, R.E., Stromberg, J.C., 1997. The natural flow regime. BioScience 47, 769–784.

Rathburn, S.L., Shahverdian, S.M., Ryan, S.E., 2017. Post-disturbance sediment recovery: Implications for watershed resilience. Geomorphology 305, 61–75. https://doi.org/10.1016/j.geomorph.2017.08.039.

Reneau, S.L., Katzman, D., Kuyumjian, G.A., Lavine, A., Malmon, D.V., 2007. Sediment delivery after a wildfire. Geology 35, 151–154. https://doi.org/10.1130/G23288A.1.

Rhoades, C.C., Entwistle, D., Butler, D., 2011. The influence of wildfire extent and severity on streamwater chemistry, sediment and temperature following the Hayman Fire, Colorado. International of Wildland Fire 20, 430–442. https://doi.org/10.1071/WF09086.

Robichaud, P.R., Beyers, J.L., Neary, D.G., 2000. Evaluating the effectiveness of postfire rehabilitation treatments. USDA Forest Service, RMRS-GTR-63, Fort Collins, CO.

Rocca, M.E., Brown, P.M., MacDonald, L.H., Carrico, C.M., 2014. Climate change impacts on fire regimes and key ecosystem services in Rocky Mountain forests. For. Ecol. Manag. 327, 290–305. https://doi.org/10.1016/j.foreco.2014.04.005.

Roering, J.J., Gerber, M., 2005. Fire and the evolution of steep, soil-mantled landscapes. Geology 33, 349–352. https://doi.org/10.1130/G21260.1.

Schmeer, S.R., 2014. Post-fire erosion response and recovery, High Park Fire, Colorado. Master's thesis. Department of Ecosystem Science and Sustainability, Colorado State University, Fort Collins, CO, p. 153.

Schmeer, S.R., Kampf, S.K., MacDonald, L.H., Hewitt, J., Wilson, C., 2018. Empirical models of annual post-fire erosion on mulched and unmulched hillslopes. Catena 163, 276–287. https://doi.org/10.1016/j.catena.2017.12.029.

Schumm, S.A., 1973. Geomorphic thresholds and complex response of drainage systems. Fluvial Geomorphology 6, 69–85.

Schumm, S.A., 1979. Geomorphic thresholds: the concept and its applications. Trans. Inst. Br. Geogr. 4, 485–515.

Schumm, S.A., 1998. To Interpret the Earth: Ten ways to be wrong. Cambridge University Press.

Schumm, S.A., Lichty, R.W., 1963. Channel widening and flood-plain construction along Cimarron River in southwestern Kansas. US Geological Survey Professional Paper 352-D.

Scott, D.F., Van Wyk, D.B., 1990. The effects of wildfire on soil wettability and hydrological behaviour of an afforested catchment. Journal of Hydrology 121, 239–256. https://doi.org/10.1016/0022-1694(90)90234-O.

Scott, D.N., Brogan, D.J., Lininger, K.B., Schook, D.M., Daugherty, E.E., Sparacino, M.S., Patton, A.I., 2016. Evaluating survey instruments and methods in a steep channel. Geomorphology 273, 236–243. https://doi.org/10.1016/j.geomorph.2016.08.020.

Shahverdian, S.M., 2015. Controls on post-High Park Fire channel response, South Fork Cache la Poudre Basin, Colorado. Master's thesis. Department of Geosciences, Colorado State University, Fort Collins, CO, p. 104.

Shakesby, R.A., Doerr, S.H., 2006. Wildfire as a hydrological and geomorphological agent. Earth Sci. Rev. 74, 269–307.

Smith, H.G., Sheridan, G.J., Lane, P.N., Nyman, P., Haydon, S., 2011. Wildfire effects on water quality in forest catchments: a review with implications for water supply. J. Hydrol. 396, 170–192. https://doi.org/10.1016/j.jhydrol.2010.10.043.

Soil Survey Staff, 2018. Natural Resources Conservation Service, United States Department of Agriculture. Web Soil Survey (Accessed: 2018-01-25).

Sosa-Pérez, G., MacDonald, L.H., 2017. Reductions in road sediment production and road-stream connectivity from two decommissioning treatments. For. Ecol. Manag. 398, 116–129. https://doi.org/10.1016/j.foreco.2017.04.031.

Surian, N., Righini, M., Lucía, A., Nardi, L., Amponsah, W., Benvenuti, M., Borga, M., Cavalli, M., Comiti, F., Marchi, L., Rinaldi, M., 2016. Channel response to extreme floods: insights on controlling factors from six mountain rivers in northern Apennines, Italy. Geomorphology 272, 78–91. https://doi.org/10.1016/j.geomorph.2016.02.002.

Swanson, F.J., 1981. Fire and geomorphic processes. In: Mooney, H., Bonnicksen, T., Christensen, N., Lotan, J., Reiners, W. (Eds.), Fire Regime and Ecosystem Properties. United States Department of Agriculture Forest Service General Technical Report WO-26, pp. 401–444.

Tabacchi, E., Steiger, J., Corenblit, D., Monaghan, M.T., Planty-Tabacchi, A.M., 2009. Implications of biological and physical diversity for resilience and resistance patterns within Highly Dynamic River Systems. Aquatic Sciences-Research Across Boundaries 71, 279–289. https://doi.org/10.1007/s00027-009-9195-1.

Thomas, M.F., 2001. Landscape sensitivity in time and space – an introduction. Catena 42, 83–98. https://doi.org/10.1016/S0341-8162(00)00133-8.

Veblen, T.T., Kitzberger, T., Donnegan, J., 2000. Climatic and human influences on fire regimes in ponderosa pine forests in the Colorado Front Range. Ecol. Appl. 10, 1178–1195. https://doi.org/10.1890/1051-0761(2000)010[1178:CAHIOF]2.0.CO;2.

Wagenbrenner, J.W., Robichaud, P.R., 2014. Post-fire bedload sediment delivery across spatial scales in the interior western United States. Earth Surf. Process. Landf. 39, 865–876. https://doi.org/10.1002/esp.3488.

Wagenbrenner, J., MacDonald, L., Rough, D., 2006. Effectiveness of three post-fire rehabilitation treatments in the Colorado Front Range. Hydrol. Process. 20, 2989–3006. https://doi.org/10.1002/hyp.6146.

Walling, D.E., 1983. The sediment delivery problem. J. Hydrol. 65, 209–237. https://doi.org/10.1016/0022-1694(83)90217-2.

Westerling, A.L., Hidalgo, H.G., Cayan, D.R., Swetnam, T.W., 2006. Warming and earlier spring increase western U.S. forest wildfire activity. Science 313, 940–943. https://doi.org/10.1126/science.1128834.

Wicherski, W., Dethier, D.P., Ouimet, W.B., 2017. Erosion and channel changes due to extreme flooding in the Fourmile Creek catchment, Colorado. Geomorphology 294, 87–98. https://doi.org/10.1016/j.geomorph.2017.03.030.

Wohl, E., 2013. Migration of channel heads following wildfire in the Colorado Front Range, USA. Earth Surf. Process. Landf. 38, 1049–1053. https://doi.org/10.1002/esp.3429.

Wohl, E.E., Pearthree, P.P., 1991. Debris flows as geomorphic agents in the Huachuca Mountains of southeastern Arizona. Geomorphology 4, 273–292. https://doi.org/10.1016/0169-555X(91)90010-8.

Wohl, E., Scott, D.N., 2017. Transience of channel head locations following disturbance. Earth Surf. Process. Landf. 42. https://doi.org/10.1002/esp.4124.

Wohl, E., Bledsoe, B.P., Jacobson, R.B., Poff, N.L., Rathburn, S.L., Walters, D.M., Wilcox, A.C., 2015. The natural sediment regime in rivers: broadening the foundation for ecosystem management. BioScience 65, 358–371. https://doi.org/10.1093/biosci/biv002.

Wolman, M.G., 1954. A method of sampling coarse river-bed material. EOS Trans. Am. Geophys. Union 35, 951–956. https://doi.org/10.1029/TR035i006p00951.

Wolman, M.G., Eiler, J.P., 1958. Reconnaissance study of erosion and deposition produced by the flood of August 1955 in Connecticut. EOS Trans. Am. Geophys. Union 39, 1–14. https://doi.org/10.1029/TR039i001p00001.

Wolman, M.G., Gerson, R., 1978. Relative scales of time and effectiveness of climate in watershed geomorphology. Earth Surf. Process. Landf. 3, 189–208. https://doi.org/10.1002/esp.3290030207.

Wolman, M.G., Miller, J.P., 1960. Magnitude and frequency of forces in geomorphic processes. The Journal of Geology 68, 54–74. https://doi.org/10.1086/626637.

Wondzell, S.M., King, J.G., 2003. Postfire erosional processes in the Pacific Northwest and Rocky Mountain regions. For. Ecol. Manag. 178, 75–87.

Writer, J.H., Hohner, A., Oropeza, J., Schmidt, A., Cawley, K.M., Rosario-Ortiz, F.L., et al., 2014. Water treatment implications after the High Park wildfire, Colorado. J. Am. Water Works Assoc. 106, E189–E199. https://doi.org/10.5942/jawwa.2014.106.0055.

Yochum, S.E., 2015. Colorado Front Range flood of 2013: Peak flows and flood frequencies. 3rd Joint Federal Interagency Conference on Sedimentation and Hydrologic Modeling, pp. 537–548.

Yochum, S.E., Sholtes, J.S., Scott, J.A., Bledsoe, B.P., 2017. Stream power framework for predicting geomorphic change: The 2013 Colorado Front Range flood. Geomorphology 292, 178–192. https://doi.org/10.1016/j.geomorph.2017.03.004.